UNIVERSITAT POLITÈCNICA DE CATALUNYA BARCELONATECH

Self-cleaning optical surfaces for the inkjet and 3D printing industry

Mehmet Alican Noyan

ICFO-INSTITUT DE CIÈNCIES FOTÒNIQUES
&
UPC-UNIVERSITAT POLITÈCNICA DE CATALUNYA

Self-cleaning optical surfaces for the inkjet and 3D printing industry

Mehmet Alican Noyan

Thesis advisor: Prof. Valerio Pruneri

PhD Thesis - 2017

to my family and friends

Abstract

Liquid and solid repellent surfaces are key to many industries. For example, construction industry benefits from self-cleaning windows, cements, paints, roof tiles, and corrosion resistant surfaces, while easy-to-clean, antifingerprint and antibacterial surfaces are highly relevant for display applications.

In inkjet and 3D printers, the unwanted deposition on the inner parts of raw materials in the form of liquid, aerosol or solid particulates may cause device malfunctioning. In particular, ink aerosol and powder may obstruct light passage in several key components, such as sensors and lamps. To address this, the thesis proposes and investigates novel designs and methods to reduce ink aerosol and powder contamination on transparent surfaces.

In the first part, Joule heating and hydrophobicity against ink aerosol contamination are studied. The former effect is provided by a transparent conducting film (TCF), while the latter through a self-assembled monolayer (SAM) coating. The combination of the two effects reduce transmittance loss from an average of 10% to less than 1.5% in the presence of ink aerosol. Correspondingly, the area of the surface covered by ink decreases from around 45% to less than 2%. Results obtained with the glass substrates are subsequently extended to the plastic window of a commercial inkjet printer calibration sensor. Furthermore, effectiveness of the proposed self-cleaning surfaces inside

an inkjet printer is demonstrated.

In the second part, a technology called “electric curtain” is used to design a self-cleaning surface against powder contamination in 3D printers. Powders are the starting material for forming the objects and are largely present inside the printer. It is shown that an electric curtain can clean about 50% of the powder that deposits on the surface . The thesis also proposes a new electric curtain design consisting of a double electrode layer which significantly increases the particle removal efficacy to more than 70%, with plenty of margin of improvement.

In summary, in this thesis novel self-cleaning transparent surfaces are proposed and their potential for inkjet and 3D printing industry is demonstrated in real operating conditions.

Resumen

En la actualidad, el uso de superficies repelentes de partículas sólidas y líquidas es de gran importancia en el ámbito de la industria. Un caso concreto es el de la industria de la construcción, donde el uso de ventanas, cementos, pinturas y tejas que son 'autolimpiables' junto con superficies resistentes a la corrosión son de gran utilidad. Asimismo, superficies fáciles de limpiar, antibacterianas y antihuella son de vital importancia para aplicaciones de visualización. En el caso concreto de las impresoras de tinta y 3D puede existir la deposición de partículas líquidas y sólidas respectivamente, durante el funcionamiento de los equipos. Esto conlleva a un mal funcionamiento de las mismas ya que, tanto el aerosol procedente de las tintas como el polvo utilizado en las impresoras 3D, pueden obstruir el paso de la luz en los componentes principales de la impresora, como son los sensores y lámparas. Con el fin de solucionar las cuestiones descritas previamente, en esta tesis se ha desarrollado un nuevo diseño y procedimiento para reducir la contaminación provocada por los aerosoles y el polvo.

En la primera parte, se estudia la reducción de la contaminación de aerosoles en el sensor de la impresora mediante dos vías, el calentamiento del mismo por efecto Joule y modificando químicamente la superficie del sensor transformándola en hidrofóbica. El efecto Joule se proporciona a través de una película conductora transparente (TCF), mientras que la hidrofobicidad se confiere mediante un revestimiento

de monocapa autoensamblada (SAM). La combinación de ambos efectos hace que la pérdida de transmisión se reduzca de un 10% a un valor igual o inferior del 1.5%. Asimismo, el área recubierta por el aerosol disminuye de un 45% a un valor de 2%. Estos resultados obtenidos para substratos de vidrio se aplicaron posteriormente a una ventana de plástico de un sensor comercial utilizado en impresoras de tinta. Finalmente, se demuestra la efectividad del proceso propuesto (efecto Joule y SAM) al instalarse en una impresora industrial.

En la segunda parte, una tecnología llamada "cortina eléctrica" se utiliza para diseñar una superficie de autolimpieza contra la contaminación de polvo en impresoras 3D. Los polvos son el material de partida para formar los objetos y están en gran parte presentes dentro de la impresora. Se muestra que una cortina eléctrica puede limpiar aproximadamente el 50% del polvo que se deposita en la superficie. La tesis también propone un nuevo diseño de cortina eléctrica consistente en una capa de doble electrodo que aumenta significativamente la eficacia de eliminación de partículas a más del 70%, con suficiente margen de mejora.

En resumen, en esta tesis se proponen nuevas superficies transparentes de autolimpieza y se demuestra su potencial para la industria de impresión por inyección y 3D en condiciones reales de funcionamiento.

Acknowledgements

I consider it my privilege to acknowledge the help, assistance and support of the many individuals without whom this thesis would not have been possible.

First of all, I would like to express my sincere gratitude to my thesis supervisor Prof. Valerio Pruneri for his guidance and continuous support during the course of this thesis.

I would like to thank Vittoria, Waldimar, Kavitha, Roland, Rinu, Dhriti, Vahagn, Inge, Albert, Kutlu, Onur, and Zafer for their help at various points during my PhD. I would like to especially express my gratitude to Vittoria, for not expelling me from her lab even though I painted it all over with ink and powder.

Also, I would like to thank ICFO's cleanroom, mechanical workshop, electronic workshop and maintanence teams for alleviating the challenges of experimental research.

I would like to thank Denis Guilhot and Silvia Carrasco from ICFO Knowledge and Technology Transfer unit for their invaluable help and Joan Saez, Xavier Bruch, Esteve Comas, Jordi Ferran, Carles Castellsague and Bernat Poll Crespo from HP Barcelona for their continuous support during our collaboration.

Personally, I would like to thank all OPTO and ICFO friends for making my life in Barcelona much more pleasant. It has been an amazing experience.

Finally, I am grateful to my lovely sister Aslı and my parents for their love and support and to my dear İnci, for everything.

Contents

List of Figures

List of Tables

List of Publications

Publications included in this thesis

Journal Articles

- M. A. Noyan, D. Guilhot, V. Pruneri, ‘‘Functionalized transparent surfaces with enhanced self-cleaning against ink aerosol contamination” *Adv. Mater. Technol.* 2, 1600113, 2016.

Patents

- V. Pruneri, M. A. Noyan, ‘‘Ink aerosol removal from a surface through heating and hydrophobicity”, Invention disclosure, 2016.

- V. Pruneri, M. A. Noyan, Filed patent application, 2017.

Other relevant publications and conference contributions

Journal Articles

- J. A. Zielinska, A. Zukauskas, C. Canalias, M. A. Noyan, M. W. Mitchell, ‘‘Fully-resonant, tunable, monolithic frequency conver-

sion as a coherent UVA source" *Opt. Express* 25, 1142-1150, 2017.

Talks

- M. A. Noyan, K. K. Gopalan, R. A. Maniyara, M. M. Martin-Frances, V. Mkhitaryan, J. Rombaut Segarra, M. Rude, R. Sibilo, I. Mannelli, J. Canet Ferrer, V. Pruneri, ''Multifunctional nanostructured optical surfaces for industrial applications" Nanometa 2017, Seefeld, Austria, January 2017 (**invited talk**).

- M. A. Noyan, V. Pruneri, ''Liquid and aerosol repellent transparent surfaces for ink-jet printing applications", 5th International Conference on Multifunctional, Hybrid and Nanomaterials, Lisbon, Portugal, March 2017 (**oral presentation**).

Chapter 1

Introduction

With the advent of nanotechnology, our ability to tailor surfaces has grown rapidly. This has lead to significant developments in self-cleaning surfaces. These surfaces have proved to be useful in a wide range of areas from labor saving applications, such as self-cleaning windows, to life saving application of antibacterial surfaces. Commercial products have been available for a while now, but their full potential has yet to be harnessed. A recent report expects rapid growth in the market for self-cleaning surfaces market, and, in particular, predicts the total market value to reach $3.3 billion by 2020 (Figure 1.1). The main focus of this thesis is the development of novel self-cleaning structures for inkjet and 3D printers, demonstrating yet another industry that can benefit from this technology.

1.1 Self-cleaning surfaces overview

A self-cleaning surface is a surface capable of reducing or preventing the occurrence of any type of unwanted matter. This matter could be anything, such as a dust particles or a bacteria, or could even be a

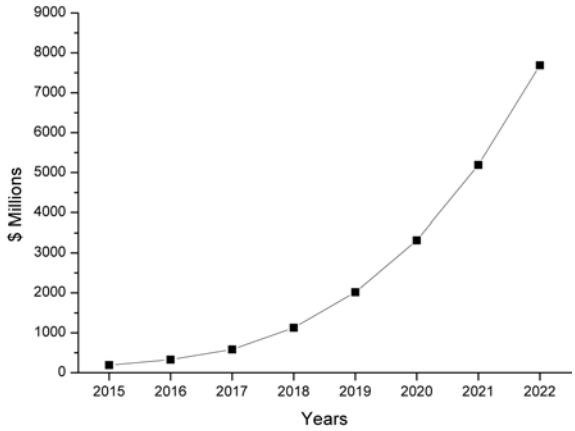

Figure 1.1: Total market forecast for self-cleaning surfaces (n-tech research 2015 [1]).

phase such as corrosion or ice. Examples of these surfaces can be readily found in nature and, therefore, biomimicry has played an important role in the development of self-cleaning surfaces. A botanist named Wilhelm Barthlott and his team at the University of Bonn discovered that structural features on plant leaves, combined with their waxy surface chemistry, result in a non-wettable surface, i.e. a hydrophobic surface. Dirt particles are picked up by rolling water droplets and are cleaned off the surface [5, 6]. The team fabricated surfaces mimicking these plant leaves and, noticing their industrial potential, patented the idea and trademarked it as "Lotus Effect®" [7]. So far, hydrophobicity has helped in the realization of self-cleaning windows, cements, paints and roof tiles.

The opposite of hydrophobicity is hydrophilicity, whereby water wets the surfaces almost completely. These surfaces can clean themselves due to water entering beneath the particles and detaching the particles from the surface. There are products on the market which

combine hydrophilicity with photocatalysis in order to improve the cleaning performance. In 2001, glass manufacturer Pilkington announced the first commercial self-cleaning product Pilkington Activ™. This is a window designed for homeowners which is capable of cleaning the dirt accumulating on itself. The window is coated with TiO_2 and, on contact with sunlight, the coating chemically breaks down the dirt on the window via the process of photocatalysis. Later, upon raining, water forms a layer on the surface, washing away the decomposed dirt particles.

Mature hydrophobic and hydrophilic technologies dominate today's market for self-cleaning materials. As well as the self-cleaning architectural components mentioned above, another area where these technologies are used is self-cleaning fibers and fabrics. This might reduce the world's water consumption, helping us to preserve our environment. In addition, hydrophobic surfaces also present opportunities to prevent corrosion. There are many other self-cleaning surfaces, however, not based on hydrophobic and hydrophilic technologies alone and their market share is expected to increase in the following years [1].

One important example of the above is antibacterial surfaces. These surfaces are indispensable for the medical industry as they are used in many components interacting with the human body. The food industry also benefits from these surfaces as the antibacterial performance of food packing is critical for conserving food. There are various working principles behind anti-bacterial surfaces; for example, their topographies are designed such that they can disrupt the cell membrane, killing the bacteria [8]. Another mechanism depends on metals being lethal to cells. Studies indicate that different metals create different kinds of damages due to oxidative stress, protein dysfunction or membrane damage [9].

Anti-icing surfaces are also important because ice on roads, aeroplane wings and windows, as well as icicles, might be dangerous to human life. Some of these surfaces are thermally driven [10]. For ex-

ample, an indium tin oxide (ITO) defrosting coating is used for some aircrafts' cockpit windows. When a current passes through the ITO, it provides heat due to Joule heating and defrosts the window.

Dust repellent surfaces are another type of self-cleaning surface. This technology is important, for example, for solar cells as dust contamination can decrease conversion efficiency. As explained previously, hydrophobic and hydrophilic surfaces can be used to clean dust particles but they depend on water being abundant. However, this is not the case for arid regions and in space. To overcome this limitation, a surface that can clean dust using an electrostatic action was developed. A set of electrodes creates alternating electric fields on the surface and causes dust particles to move away dust. This is called an electric curtain or electrodynamic screen [11].

1.2 Aim of the thesis

This thesis has been devoted to the development of self-cleaning surfaces for inkjet and 3D printers in order to deal with contamination of critical printer parts. The self-cleaning properties of these parts would increase their lifespan. This project has been an industrial project in collaboration with an industrial partner, Hewlett-Packard Barcelona. Surfaces validated in the laboratory were tested on-site, inside the printers at Hewlett-Packard Barcelona.

The first objective of this thesis is to develop a transparent surface capable of reducing or preventing ink aerosol contamination generated inside inkjet printers. For this, a surface combining Joule heating and hydrophobicity has been designed. The second objective is to design a transparent surface for 3D printers with the ability to clean the powder which contaminates the printer parts. For this, an "electric curtain", consisting in surface electric fields applied through properly designed multilayer co-planar electrodes, was used.

For both surfaces, the aim has been to fabricate corresponding samples, to build a deposition system to create the contamination, to apply the cleaning procedure and finally to develop a characterization protocol to quantify the effect of cleaning.

Last but not least, objective in both cases has been to ensure industrial applicability. This has been achieved by using identical substrates and contaminants as the ones utilized in the printers and by further testing of the surfaces inside the printers.

1.3 Thesis outline

The thesis can be divided into two parts. The first part (Chapters 2 and 3) describes the self-cleaning surfaces for inkjet printers and the second part (Chapters 4 and 5) presents the self-cleaning surfaces for 3D printers. Including the introduction (Chapter 1) and conclusions (Chapter 6), there are six chapters in total.

In the first part, Chapter 2 starts by describing the ink aerosol contamination problem, and stating conventional solutions proposed and the solution presented in this work. Later, basic principles of Joule heating and wettability of liquids on flat surfaces are described. The chapter goes on to explain the details of fabrication, testing and characterization of the self-cleaning structures against ink aerosol contamination. The chapter ends with a discussion of the obtained results. Chapter 3 presents the testing of the surfaces explained in Chapter 2. The experimental procedures and results are explained and discussed in detail.

In the second part, Chapter 4 tests the effectiveness of the electric curtain technology against the powder used in 3D printing. The chapter starts by explaining how this powder contamination is formed and describes what problems it poses. It goes on to explain the various powder removal efforts studied so far. Before going into the ex-

perimental details, a brief background on particle adhesion and the electric curtain is presented. Then fabrication,testing and characterization methods are given in detail and, finally, the results are shown and discussed. Chapter 5 introduces a novel structure, a double layer electric curtain, which further improves the self-cleaning performance over a single layer electric curtain. It describes the structure in detail and how its performance is characterized. Later, simulations and testing of the several double layer electric curtain configurations are given and compared with a single layer electric curtain.

Finally, Chapter 6 summarizes the results and presents an outlook for future directions.

Chapter 2

Self-cleaning surfaces for inkjet printing

2.1 Introduction

Aerosol is the name given to small particles (solid or liquid) suspended in air (or any other gas), and it can be seen in nature. Fog, for example, is a natural aerosol made up of small water droplets. Volcanic aerosol and desert dust are other examples of natural aerosol. They affect our planet's atmosphere significantly. Aerosols are generated artificially, too. They are used in medical treatments for respiratory illnesses, in sprays to deliver consumer products such as deodorant and paint, and also in agriculture for pesticide delivery. Ink aerosol forms inside inkjet printers, the most common printer type on the market today, as an unwanted side effect of printing.

Inkjet printing is used extensively for printing text and images onto substrates, but it is also used for printing electronics, optical devices and biological arrays [12–16]. The basic principle of inkjet printing is to fire ink droplets generated through the application of a pulse of

pressure, through a set of nozzles and onto a substrate (paper, plastic, etc.) in order to create the pixels of the intended image [17]. The ink is made of a colorant (e.g. pigment, dye) and a vehicle (e.g. water, organic solvent). The ink droplets in the aerosol can originate from two main mechanisms: (i) dispersion into the surrounding air of larger printing droplets flying from the printhead to the paper, and (ii) the droplets themselves, when tiny enough to get incorporated into the aerosol.

To prevent ink drying on the nozzles, printheads clean them by spraying excess ink into a separate component called a spittoon. This action is an important source of aerosol generation. The aerosol generation issue is more critical in large format printers, as these are high performance machines consuming significant amounts of ink compared to desktop printers.

Ink aerosol can accumulate on the mechanical components, which may get in contact with the printing media, hence decreasing the quality of the image. It can also accumulate on encoder strips, causing false readings and, eventually, failures. However, the most significant detrimental effect of ink aerosol is the contamination of the transparent windows of the optical sensors, one of which is a multi-purpose sensor used for calibration of the printhead position, and also the color and media advanced systems (Figure 2.1). Aerosol deposition on this photo-detector protection window reduces transparency and prevents the light from reaching the sensor, which affects its functional performance.

Several approaches have been proposed in order to reduce the effects associated with ink aerosol contamination, for example optimizing designs and algorithms to reduce the amount of ink generated [18] or to increase its collection while it flies around inside the printer chamber [19]. However, these methods are holistic i.e. they reduce aerosol contamination on critical parts as well as non-critical parts. An approach addressing the issue of aerosol contamination on specific

(a) (b)

Figure 2.1: a) Calibration sensor used in HP inkjet printers. b) Printer during color calibration

parts would save energy.

This part of the thesis focuses on designing and developing functionalized surfaces that can prevent and reduce ink aerosol contamination. Figure 2.2 depicts the proposed surface functionalization approaches. First, transparent conducting films (TCFs) were used in order to heat up the surface of a transparent substrate using electrical currents (Joule effect). In this way, liquid ink vehicle droplets that were in contact with the surface evaporate. Secondly, we applied a low surface tension self-assembled monolayer (SAM) to achieve hydrophobic surfaces. Such surfaces have large contact angles that prevent the spreading of the droplets, thus reducing the area shadowed by the ink aerosol and thereby increasing wavelength-dependent transparency. Moreover, vehicle and colorant slippage are more likely thanks to the lower sliding angle. While it is known that functionalized surfaces with TCF or SAM can repel liquids [20], they have never been applied to ink aerosol or in a demanding environment such as that of a high-throughput printer. Thirdly, for the first time, we combined Joule heating and hydrophobicity to further enhance the self-cleaning properties provided by the two methods separately. A combination

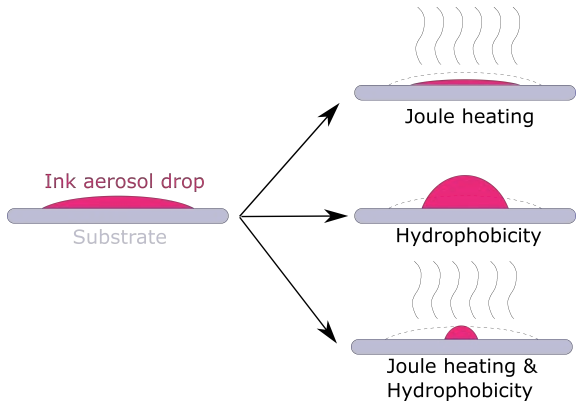

Figure 2.2: A simple schematic visualization of the concept proposed to reduce ink aerosol contamination

of a TCF and a SAM has been reported before, but the aim of that work was to protect the TCF from environmental degradation using the SAM [21]. Heating or self-cleaning were not involved.

2.2 Background

In this section, a brief background on Joule heating, wetting and self-assembled monolayers are given.

2.2.1 Joule heating

When an electric current passes through a conductor, heat is produced. This phenomenon is called Joule heating (also, ohmic or resistive heating) and it was first described by James Prescott Joule in 1840. He did several experiments involving a wire immersed in water and measured the temperature rise caused by a current passing through the wire. He deduced that the heat produced was proportional to the square of the

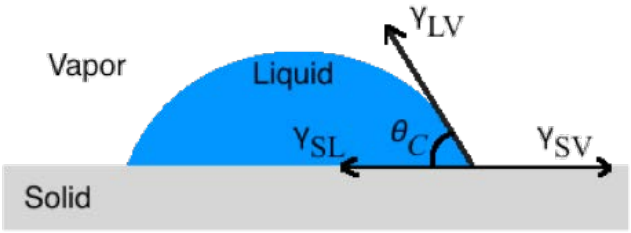

Figure 2.3: Contact angle, θ_c, the measure of wettability.

current multiplied by the resistance of the wire. The heating is caused by particle collisions during current passage.

Combined with Ohm's law (V=IR), the equations describing Joule heating can be given as:

$$P = I^2R = IV = V^2/R \tag{2.1}$$

where P is the power in watts (W), I is the current in amperes (A), R is the resistance in ohms (Ω) and V is the potential difference in volts (V).

2.2.2 Basics of wetting

The wettability of liquids on flat, homogeneous surfaces depends on the interfacial energies between the vapor, liquid and solid phases. The measure of wettability is the contact angle. It is the angle between the liquid/solid and liquid/vapor interface at the three-phase boundary point (Figure 2.3).

Young's equation (Equation 2.2) gives the relation between interfacial tensions and the contact angle. Therefore, the contact angle is also referred as Young's contact angle [22].

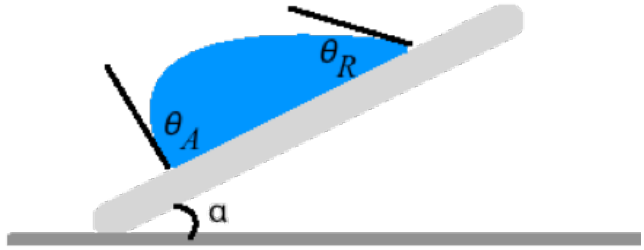

Figure 2.4: Sliding angle(α), advancing contact angle(θ_A) and receding contact angle(θ_R).

$$\gamma_{SL} + \gamma_{LV} cos\theta_c = \gamma_{SV} \tag{2.2}$$

If the contact angle is less than 90°, it is said that the liquid wets the surface (philic) whereas if the contact angle is greater than 90°the surface is non-wetting (phobic). Water is the most common liquid used for the measurements, and, therefore, the contact angle of water on a surface is given a specific name, which is the water-contact-angle (WCA). If the WCA is less than 90°, the surface is termed hydrophilic, if it is more than 90°, the surface is hydrophobic and, finally, if the WCA is more than 150°, then the surface is called superhydrophobic.

The other important wetting merit is the tilting (or sliding) angle (Figure 2.4). This is the tilt angle of a surface where the droplet starts to slide. The difference between the advancing and the receding angle gives the contact angle hysteresis. On slippery surfaces, the sliding angle and contact angle hysteresis are low.

2.2.3 Self-assembled monolayer (SAM)

To change wetting properties of surfaces, self-assembled monolayers (SAM) are typically used. They are molecular chains which spointaneously grow on surfaces. They consist of a head group which forms the chemical bond with the surface of the substrate and ending with a terminal group (Figure 2.5a).

SAMs modify the surface chemistry so that one can obtain more wetting or less wetting of liquids. For a given liquid and vapor, say water and air, degree of wetting is governed by the surface energy of the substrate (Figure 2.3, Equation 2.2). If the surface energy of the substrate is high, liquid would wet the surface (philic), whereas, if the surface energy of the substrate is low, liquid would not wet the surface (phobic). Phobic or philic surfaces could be obtained with SAMs by modifying their terminal groups accordingly. Figure 2.5b shows an example of a SAM. The terminal group in this case is methyl (CH_3) which makes the sample hydrophobic. Instead, alcohol (OH) or carboxyl (COOH) terminal groups could be used to obtain hydrophilic surfaces.

2.3 Methods

2.3.1 Joule Heating

The TCF for surface Joule heating was a 100 nm-thick Indium Tin Oxide (ITO) film deposited onto 25 x 25 mm^2 fused silica substrates using sputtering (AJA International ATC Orion 8 HV). After cleaning the substrate using acetone and ethanol in an ultrasonic bath, sputtering of the ITO was carried out. The substrate-target distance was set to 30 cm. When the base pressure reached 0.01 mTorr, Ar (20 sccm) and O2 (1 sccm), deposition precursor gases were introduced into the system and the deposition pressure was set to 2 mTorr. After

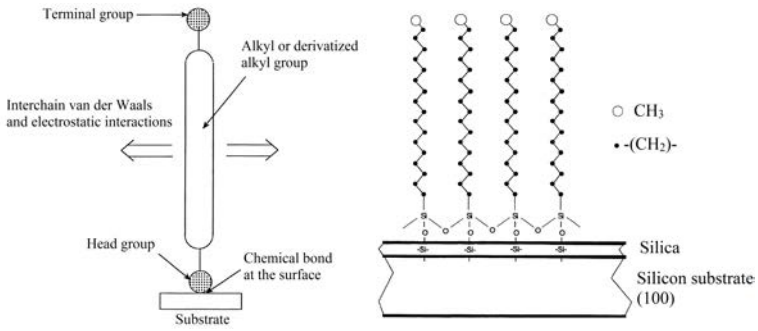

Figure 2.5: A schematic of (a) a self-assembled monolayer (SAM) on a surface and (b) an example SAM methyl-terminated, n-alkylsiloxane monolayer on Si/SiO_2. Methyl (CH_3) is a commonly used terminal group for hydrophobicity [2].

deposition of the TCF, nickel stripe electrical contacts were deposited onto the ITO to achieve a uniform current (heating) over the entire transparent surface (Figure 2.6a). A power supply (AIM-TTI Instruments EL302R) was used to apply a constant electrical current and the temperature distribution over the heated surface was measured with an IR camera (Keysight Technologies U5855A TrueIR Thermal Imager). The average temperature was kept constant between 80 °C and 85 °C for all experiments, by applying direct current of 0.27A and 9V.

The Joule heating might change optical and electrical characteristics of the ITO due to annealing [23]. This would cause inconsistencies when comparing heated and non-heated samples. Therefore, ITO films were annealed at 250 °C for 25 minutes, much higher temperature and longer time than those for the Joule heating so that no change of the ITO properties will occur during the experiments.

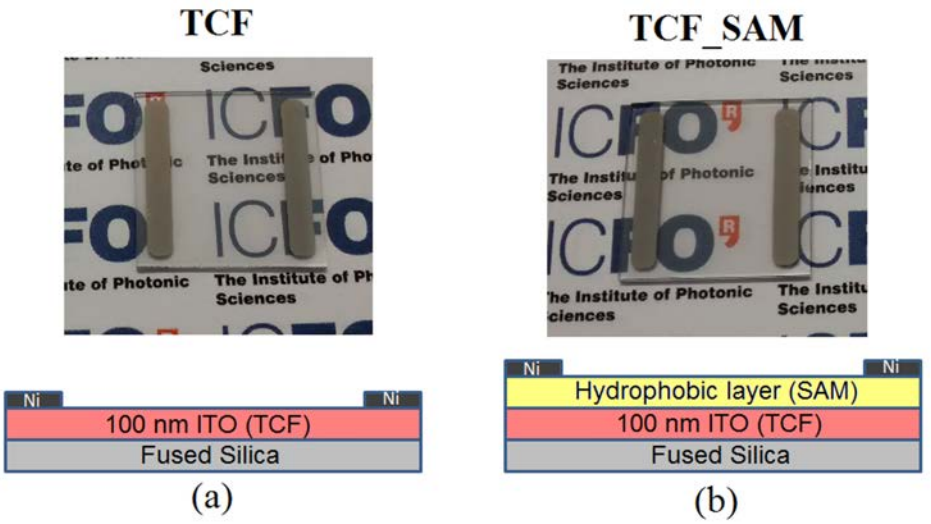

Figure 2.6: Images and cross-section schematics of the samples (a) without SAM and (b) with SAM. The effect of SAM is practically invisible as it does not significantly change the transmission of the transparent and electrically conductive surface.

2.3.2 Hydrophobicity

Samples were coated with a self-assembled monolayer (SAM), alkoxysilane functional perfluoropolyether (PFPE) hybrid polymer from Dow Corning (2634 Coating). The SAM was initially diluted to 0.1% with a fluorinated solvent (Novec HFE 7200). Substrates were dipped into the solution for 3 minutes and dried at 50 °C for 1 hr. Finally, they were rinsed in Novec HFE7200 solvent (Figure 2.6b). Contact angles and sliding angles for water and ink droplets were measured using a Krüss GmbH DSA100 drop shape analyzer.

2.3.3 Aerosol Deposition

This study required a repeatable aerosol generation and deposition system, capable of generating aerosol particles with sizes similar to the ones generated inside the printer. Early studies involving aerosols generally used custom-built aerosol generation systems and nowadays a variety of commercial aerosol generators exist [24]. In our experiments, a spray setup was built for aerosol deposition, comprising an Agar Scientific Glass microspray device. For repeatability, a purge valve and pressure controller were used instead of a hand squeeze ball pump. Holders were used to fix the microspray and the target substrate. Each sample was sprayed for 48 seconds. Electrical wiring enabled the application of an electrical current to the sample while it was in the setup. Images of the spray setup can be seen in Figure 2.7.

2.3.4 Characterization

A UV-Vis spectrophotometer (Perkin Elmer Lambda 950) was used to measure the transmittance (T%) of the samples, which can be considered a reliable quantification of the overall aerosol contamination on the samples. The measurement was carried out between 300nm and 800nm, in the sensor working range. Optical microscopy was used to analyze the ink aerosol distribution on the substrate. The images were processed using an image processing software (ImageJ), to measure the percentage of area covered by the ink aerosol (PAC, %), the number of particles per unit area (N_p/mm^2) and the average size (μm^2) of the particles. The experiments and measurements were repeated 3 times on each sample and each time (i.e. each spray) 5 images were taken from different points of the sample.

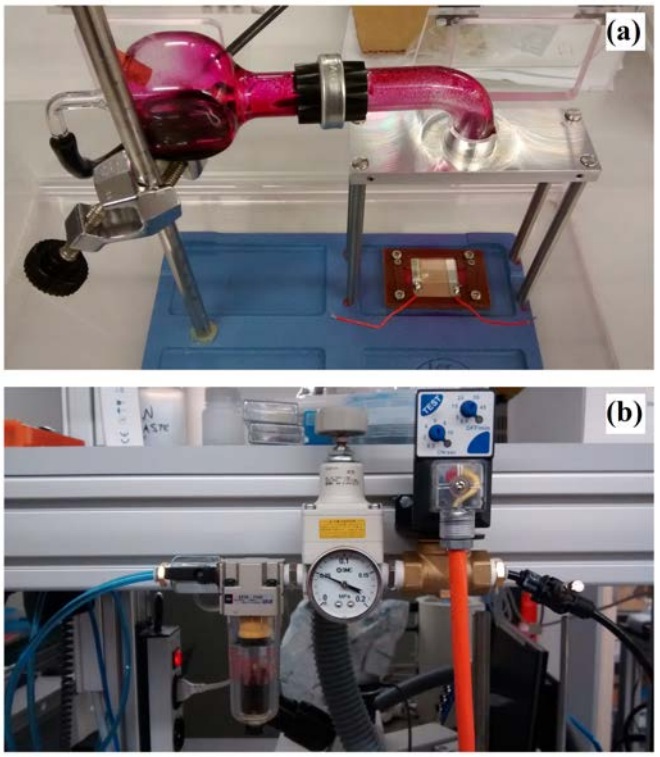

Figure 2.7: Image showing the elements of the spray setup. (a) Glass microspray and the sample to be sprayed. Both are fixed with holders for repeatability. (b) Pressure controller for fixing the spray pressure and the purge valve for fixing the spray time.

2.4 Results and discussion

First part discusses the results obtained with the substrate fused silica. Later, second section, extends the concept on to the calibration sensor window.

2.4.1 TCF and SAM on the fused silica

Before the experiments with ink aerosol, the Joule heating and hydrophobicity were characterized. For the Joule heating, an electrical current was applied to the sample using the TCF. In order to maintain the temperature of the sample between 80-85 °C, the necessary power per unit surface area was measured to be 0.64 W/cm^2. It took less than 3 minutes to reach the desired temperature. When the temperature was stabilized, heat distribution over the sample surface was observed to be uniform. Figure 2.8 shows the evolution of temperature over time upon the application of power and an IR image shows the heat distribution.

For hydrophobicity due to SAM, contact angle (CA) and sliding angle measurements were carried out for both water and ink. For the samples without SAM and with SAM, the CAs of for a 5 μL water droplet were 78°and 113°, respectively. For the ink, the three-phase boundary moved after the droplet was placed onto the surface, and, therefore, CAs at t = 0 min and t = 10 min were measured. The CAs of a 5 μL ink droplet on the samples without SAM and with SAM were 48°and 67°at t = 0 min, and 13°and 41°at t = 10 min, respectively (Figure 2.9). On the sample with SAM, the sliding angles for 8 μL and 10 μL water droplets were measured to be 42°and 22°, and for ink droplets 50°and 35°, respectively. For the same volume of water and ink droplets, no sliding was observed on the sample without SAM. The effects of SAM on absorption, reflection and transmission were negligible.

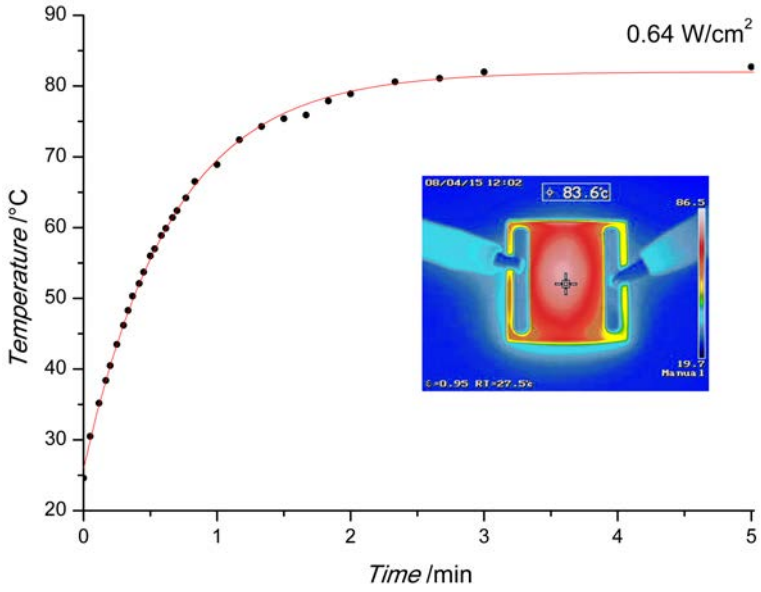

Figure 2.8: Temperature evolution of the sample upon Joule heating. The power required to keep the temperature of the sample between 80-85 °C was measured to be 0.64 W/cm^2. The sample was suspended in air during the experiment, and the ambient temperature was 27.5 °C.

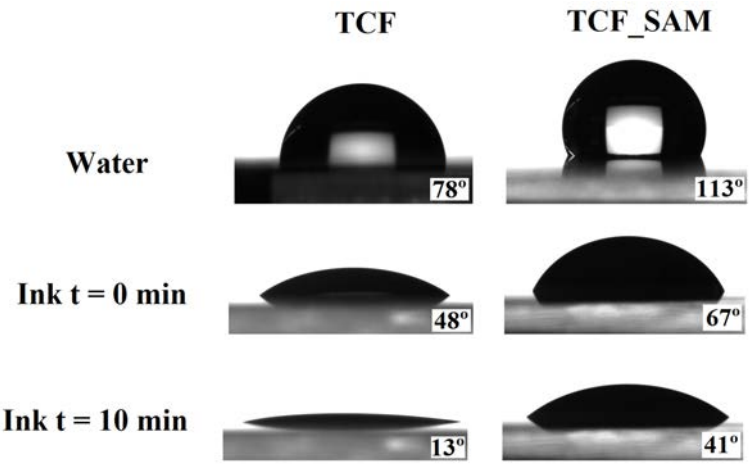

Figure 2.9: Contact angles of water and ink droplets of 5 μL on samples with and without SAM.

After the characterization of TCF Joule heating and SAM hydrophobocity, two different structures described in the methods section (Figure 2.6) were considered for ink aerosol experiments. Samples with TCF alone (Figure 2.6a) and with TCF coated with SAM (Figure 2.6b) were sprayed using an ad-hoc deposition system (see experimental section for more details). Two different Joule heating modes were considered (Figure 2.10): in the first one the samples were heated after spraying the aerosol (heating mode 1, H1) while in the second, the samples were first heated and then maintained at a given temperature during spraying (heating mode 2, H2).

Transmittance (T%) spectra of the samples are given in Figure 2.11a and light microscopy images of the samples are presented in Figure 2.11b. From the light microscopy images, the percentage of the area covered by ink (PAC), the number of particles per unit area (N_p/mm^2), and the average size (μm^2) of the particles were extracted

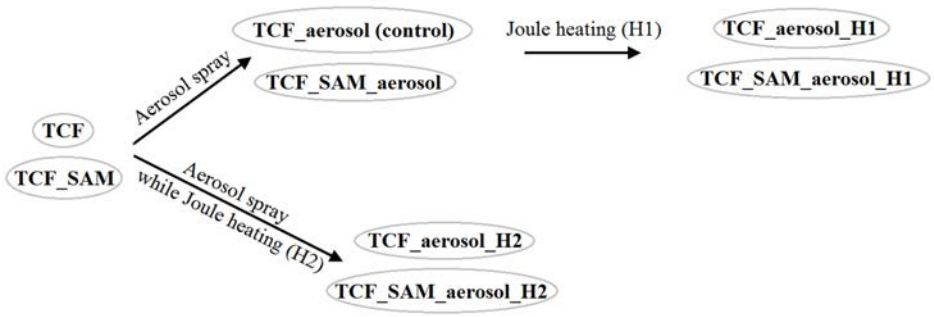

Figure 2.10: Experimental flowchart presenting the spraying and heating procedures.

using image analysis, and are presented in Table 2.1. Clearly, the figure of merit for the sensor window is T%. The more transparent the surface, the cleaner it is in terms of ink contamination. The light microscopy images were analyzed and quantitatively translated into values for further clarification of the effects of TCF and SAM on the T%.

The T% spectra of the samples reveal that the sample with SAM and subjected to heating mode 2 (TCF_SAM_aerosol_H2) is the one less prone to ink aerosol contamination. The difference in optical transmittance between TCF_SAM_aerosol_H2 and the uncontaminated bare sample (TCF) is less than 1.5%, for every wavelength in the measured spectrum. Individual effects of TCF (Joule heating) and SAM (hydrophobicity) can also be deduced from the spectrum. Firstly, for TCF, it can be seen that the Joule heating increases the transparency of the samples contaminated with ink (both with and without SAM). As explained in the experimental section, two different heating modes

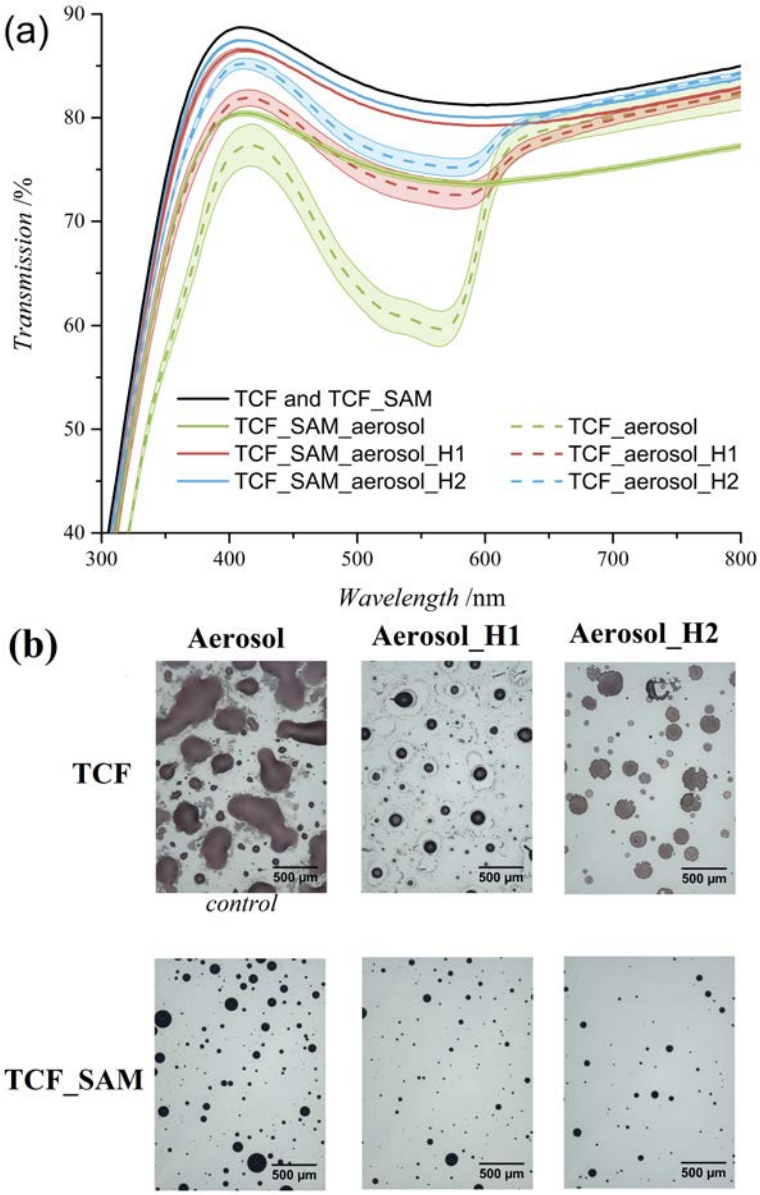

Figure 2.11: Characterization of the samples shown in the experimental flowchart. (a) Optical transmittance spectra. Fill area corresponds to the standard deviation. (b) Light microscopy images.

Table 2.1: Image processing results of the images shown in Figure 2.11b. Values indicated by plus or minus sign are standard deviations.

Sample	Area covered by ink (PAC) [%]	Particle count [N_p/mm^2]	Average size [μm^2]
TCF aerosol (control)	45.62±6.15	245.89±93.30	2052.55±643.99
TCF aerosol H1	8.33±0.51	475.40±26.58	175.35±8.58
TCF aerosol H2	15.27±2.78	27.55±4.45	5663.90±1319.66
TCF SAM aerosol	7.82±0.61	93.54±6.38	841.01±100.25
TCF SAM aerosol H1	3.04±0.37	90.06±4.52	339.88±52.76
TCF SAM aerosol H2	1.71±0.25	19.28±2.09	893.98±145.12

were used. Of these, heating mode 2 (blue curves) outperforms heating mode 1 (red curves).

Secondly, with regard to the effect of SAM, a significant difference between the samples with SAM and without SAM draws our attention: there is a specific absorbance pattern for the samples without SAM, which is absent for the samples with SAM. It is reasonable to anticipate specific absorbance from ink, because it is used to provide a specific color, but the inks used for all the experiments were the same and only in the case of samples without SAM do we observe this wavelength-specific absorption. We believe that the observed difference is related to the height of the droplets. In the case of the samples with SAM, the droplets had a larger contact angle, and, therefore, a larger average height, and acted as dark spots for the probing light. Hence, there was a wavelength-independent decrease in transparency. On the other hand, in the case of the samples without SAM, the droplets were spread over a larger area, allowing light to pass through them and consequently evidencing the colorant absorption fingerprint (Figure 2.12a). This is also consistent with the observed absorption spectra of the ink-water solution for varying ink concentrations, from 0.1% to 100% (Figure 2.12b). Above 5% ink concentration, the absorption of the ink (colorant) was no longer evident.

This means that the effect of SAM is wavelength dependent. Comparing the dotted and solid curves of the same color in Figure 2.11a, one can see that below 600 nm, the samples with SAM are more transparent than the samples without SAM. However, above 600 nm, TCF_SAM_aerosol is less transparent than TCF_aerosol, above 600 nm. For the samples with heating, SAM does not affect transparency significantly. This can be seen by comparing TCF_aerosol_H1 with TCF_SAM_aerosol_H1 and TCF_aerosol_H2 with TCF_SAM_aerosol_H2, above 600 nm.

Light microscopy images of the samples were taken and studied in order to understand the mechanisms behind the observed transmit-

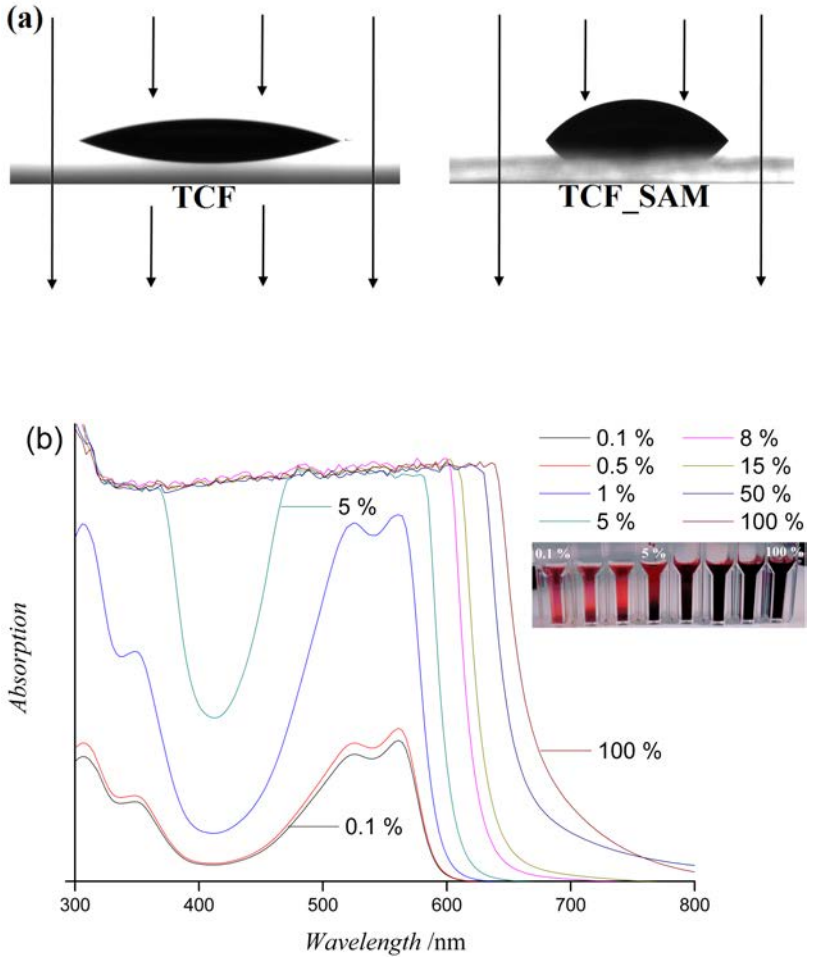

Figure 2.12: (a) Image showing light-ink drop interaction depending on the contact angle. (b) Absorption spectrum of ink-water solution for varying ink concentrations.

tance spectra. First, let us understand how heating increases the transparency of contaminated samples. Upon heating TCF_SAM_aerosol, one obtains TCF_SAM_aerosol_H1. Comparing the light microscopy images of these two samples, one can see that almost all of the ink droplets remained on the surface but they became smaller. This is confirmed by the PAC value going down from 7.82 ± 0.61 % to 3.04 ± 0.37 % while the number of particles stay almost the same. This suggests that the vehicle evaporates but the colorant stays on the surface (ink consists of a colorant and a vehicle). This can also be seen for the samples without SAM by comparing TCF_aerosol with TCF_aerosol_H1. One could observe some vehicle evaporation and colorant density increase in the centers of the ink droplets. To see the effect of the two different heating modes (H1 and H2), let us compare TCF_SAM_aerosol with TCF_SAM_aerosol_H2. The PAC value decreases from 7.82 ± 0.61 % to 1.71 ± 0.25 % but this time the number of particles does not stay the same, it goes down from 93.54 ± 6.38 to 19.28 ± 2.09. This might indicate that a large fraction of the droplets evaporated or drifted away through convection before touching the surface, and comparing the samples without SAM supports this possibility. The evaporated droplet shape (colorant concentrated on the center leaving some vehicle around the edge), which can be seen on TCF_aerosol_H1, cannot be seen on TCF_aerosol_H2. This also suggests that the droplets might have evaporated before touching the surface. This explains why heating mode 2 outperforms heating mode 1 in transmittance measurements. Heating mode 1 removes the vehicle from the surface leaving the colorant behind, whereas heating mode 2 removes the vehicle and, in addition, prevents some of the ink reaching the surface, thus decreasing the colorant on the surface.

The effect of SAM can be seen by comparing the light microscopy images of TCF_aerosol and TCF_SAM_aerosol. As anticipated, the droplet spreads more on the sample without SAM than on the sample with SAM. The PAC value goes down from 45.62 ± 6.15 % to 7.82

± 0.61 %, respectively. In other words, the sample with SAM has a larger uncontaminated area (100% – (7.82 ± 0.61%)) compared to the sample without SAM (100% - (45.62 ± 6.15%)). Hence one might expect the samples with SAM to be more transparent compared to the samples without SAM, but, as explained previously, droplets on the sample with SAM are less transparent compared to the droplets on the sample without SAM. This is due to the difference in average droplet height (Figure 2.12), and the transparency of the droplets on the sample without SAM is greatly dependent on the wavelength due to the specific absorption of the ink. This interplay between opposite forces determines the wavelength dependency of the effect of SAM observed in the transmittance measurements. Below 600 nm, the droplets on both samples TCF_SAM_aerosol and TCF_aerosol have similar opacity due to specific absorbance of the thinner droplets on TCF_aerosol. Hence the PAC determines the transparency, with a lower PAC resulting in higher transmittance values. Above 600 nm, droplets on the sample with TCF_aerosol become almost transparent. This increases the transparency of TCF_aerosol above TCF_SAM_aerosol. In addition, one can see that SAM also affects the evaporation behavior of the droplets. On TCF_aerosol_H1, there are traces of the vehicle around the remaining colorant, whereas the surrounding of the colorant on TCF_SAM_aerosol_H1 lacks visible traces of the vehicle. This is because SAM reduces the stickiness of the surface.

Transparency evolution was also observed “in situ” and Figure 2.13 shows how spraying decreased the transparency of the sample with ITO and SAM, whilst heating increased it, with a cleaning step of 50s.

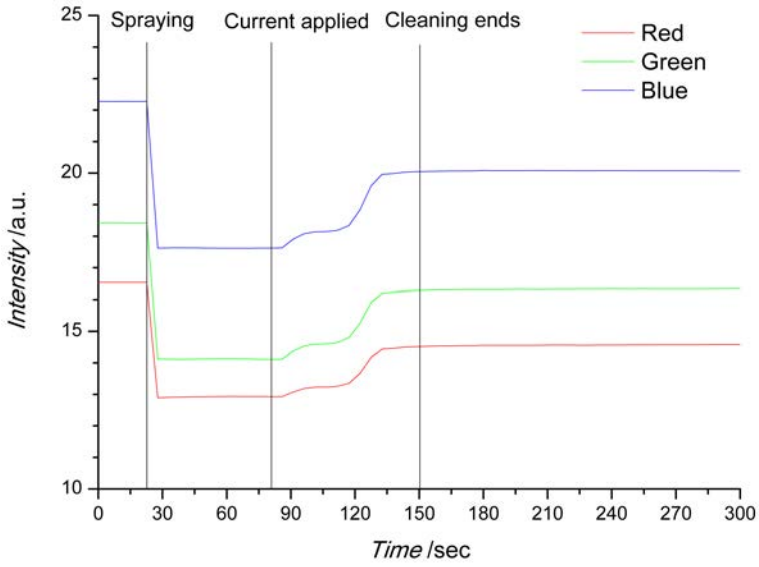

Figure 2.13: Light intensity vs. time graph showing how spraying and heating effects the detected light.

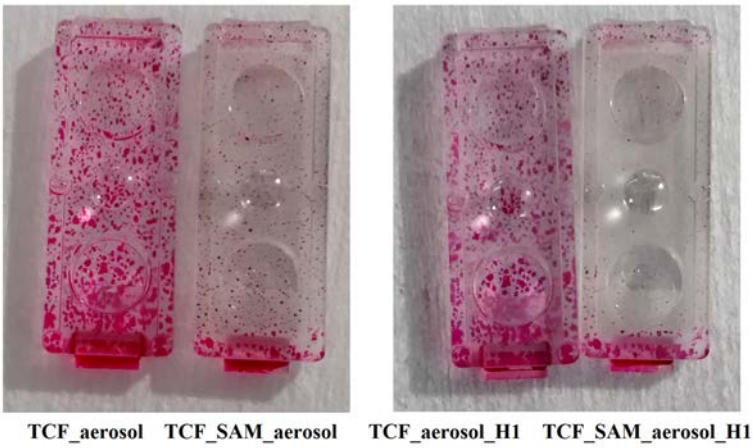

Figure 2.14: Effect of hydrophobicity and heating on the actual sensor window.

2.4.2 TCF and SAM on the calibration sensor window

The cleaning action of the TCF and SAM was demonstrated to be working on glass (fused silica). However, the window covering the calibration sensor is made of plastic (polycarbonate). TCF and SAM were deposited on to the plastic window. Figure 2.14 shows the cleaning effect on the calibration sensor window. The window curvatures and non-uniform transparency did not allow performing a characterization as precise as with the fused silica. Nevertheless, the effect was visually evident and very similar to the detailed experiments reported above: ink aerosol content was significantly decreased as a result of heating, hydrophobicity and the combination of both effects.

2.5 Conclusions

We have investigated the self-cleaning effect of transparent surfaces covered with a transparent conducting film (TCF) and a hydrophobic self-assembled monolayer (SAM) against ink aerosol contamination. The former method induced Joule heating. Even though Joule heating and hydrophobicity individually reduced ink aerosol contamination (depending on the wavelength), the experiments revealed that a combination of both methods was far more effective. Without hydrophobicty and Joule heating, the transmittance loss of the bare substrate sprayed with ink was around 10% on average and reached 20% in the specific absorption range of the ink. Transmittance loss was reduced to below 1.5% for the sprayed samples treated with both hydrophobicity and Joule heating. In addition, this treatment reduced the percentage of the area covered by ink from 45.62 $\pm$ 6.15 % to 1.71 $\pm$ 0.25 %. The results obtained with glass substrates were extended to the plastic window of an optical calibration sensor widely used in commercial inkjet printers, thus demonstrating the potential of the proposed approach to prevent and reduce aerosol contamination in real world applications.

Chapter 3

Inkjet printer test of the self-cleaning surfaces

3.1 Introduction

In the previous chapter, a transparent surface capable of reducing and preventing ink aerosol contamination was demonstrated. To simulate the ink aerosol generated inside an inkjet printer, a custom-built setup was used (see section 2.3/Aerosol deposition). The conditions inside a printer, however, aren't the same and because of this, cleaning performance of the structures might be different. For this reason, surfaces were tested inside a large format inkjet printer, and this chapter is devoted to this experiment.

Several differences between the ink aerosol generated in a laboratory and in a printer can be noted. First of all, in a printer, a set of different colors is used, which means that the specific absorbance for one color seen in the laboratory experiments is not expected within a printer setting. In addition, the size distribution and the amount of ink aerosol contamination for a given printing volume might also

Figure 3.1: The printer (HP Latex 560) used for the tests. (a) Printing area and (b) spittoon marks the regions where samples were installed during first and second tests, respectively.

vary. These values are unknown because, until now, a quantitative characterization of ink aerosol contamination has never been carried out at HP Barcelona. Finally, it should be noted that in the laboratory, aerosol from one spray is generated in approximately a minute, whereas, inside the printer, contamination is accumulated over a long time period, typically years.

3.2 Experimental details

The printer used for the test was an HP Latex 560 printer (Figure 3.1). The lifetime of printers is generally given as the total amount of ink in liters (L) consumed for printing. For this model recommended maintenance is stated as 100L and it has a lifetime of 550L.

Only heating mode 2 (H2), i.e. heating while spraying, was considered for the printer tests because the printer was continuously working.

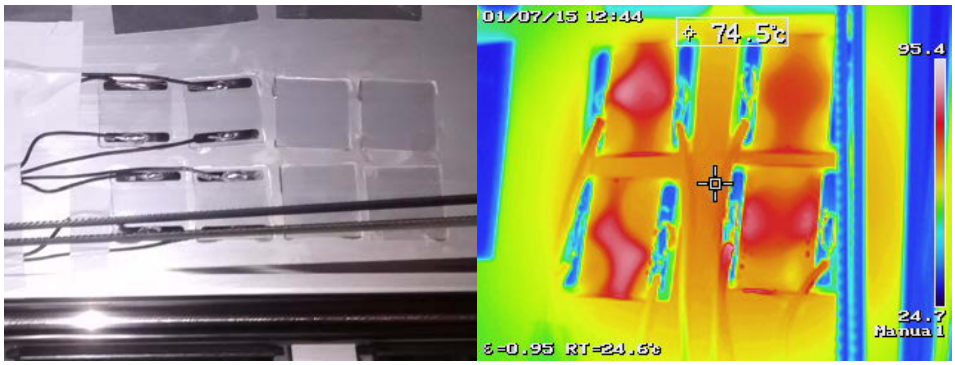

(a) (b)

Figure 3.2: First test in the printing region. (a) Sample installation. (b) IR image of the samples.

After the power supply for Joule heating was set, it was left on during the whole experiment. The tested samples were TCF_ aerosol, TCF_ SAM_ aerosol, TCF_ aerosol_ H2, and TCF_ SAM_ aerosol_ H2.

The ideal place to mount the samples would be right beside the calibration sensor. However, this sensor is inside a moving part called a printhead carrier so this would be technically very difficult because electrical wiring is required for heating the samples. Therefore, for the first experiment, the samples were placed on the metal plate behind the printhead carrier, where printing occurs (Figure 3.1a). This location was easily accessible. A direct current of 3.1A and 29V was necessary to heat the samples to around 80 °C. This is much higher than the power used in the laboratory experiments, the reason being that the metal plate behind the samples acts as a heat sink for the heated samples. The area of installation with the samples and their IR images can be seen in Figure 3.2.

In the second experiment (Figure 3.3), the samples were placed beside the spittoon (Figure 3.1b). In this region, a higher amount of

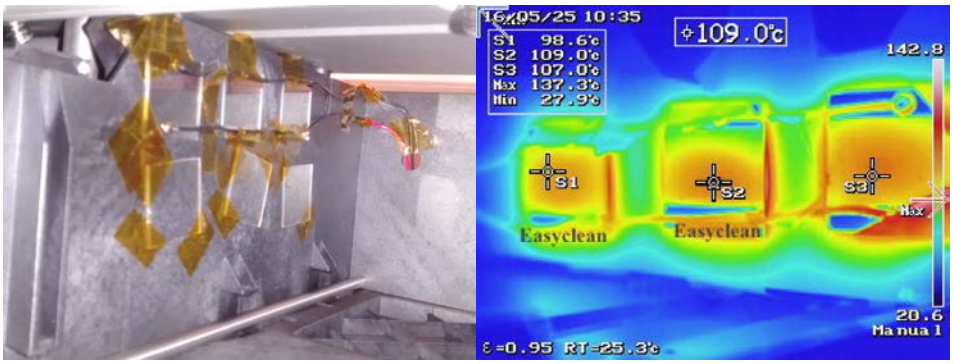

(a) (b)

Figure 3.3: Second test in the spittoon region. (a) Sample installation. (b) IR image of the samples. "Easyclean" refers to the SAM layer.

ink aerosol was expected. This time samples were placed on plastic; therefore, 9V, 0.8A DC was enough for reaching above 80 °C.

3.3 Results and Discussion

The first test ran up to 100L printing time, close to its recommended maintenance. It took 100 days to reach that level. None of the samples accumulated aerosol. From this, we can conclude that there was not enough ink aerosol generation close to the metal plate behind the printhead carriage.

For the second test, in the region of the spittoon, more aerosol generation was expected due to spitting action of the printheads. In addition, we planned to drive the printer until the end of its lifetime. At around 100L, aerosol accumulation was observed and the experiment kept running until 400L of ink had been, a total of 208 days. The T% and light microscopy images of the samples are given in Figure

Table 3.1: Image processing results of the images shown in Figure 3.4b. Values indicated by plus or minus sign are standard deviations.

Sample	Area covered by ink (PAC) [%]	Particle count [N_p/mm^2]	Average size [μm^2]
TCF aerosol (1)	6.57±2.14	37e3±8e3	1.76±0.23
TCF aerosol (2)	2.71±0.40	27e3±4e3	0.99±0.03
TCF SAM aerosol	7.11±0.55	41e3±5e3	1.74±0.11
TCF aerosol H2	0.12±0.02	446±114	2.92±0.90
TCF SAM aerosol H2 (1)	0.02±0.01	124±61	1.55±0.69
TCF SAM aerosol H2 (2)	0.08±0.04	422±19.94	109±0.51

3.4 and particle analysis of the ink content on the samples are shown in Table 3.1.

Before considering the effects of Joule heating and hydrophobicity, two important differences between the printer test and the laboratory tests should be noted, as mentioned previously in the introduction. The first one is the fact that the particle sizes for the aerosol generated inside the printer test (Table 3.1) are much smaller than for the aerosol generated in the laboratory (Table 2.1). Secondly, in the lab experiment only one color is used, whereas the actual printer uses several different colors. Therefore, as expected, a specific absorption

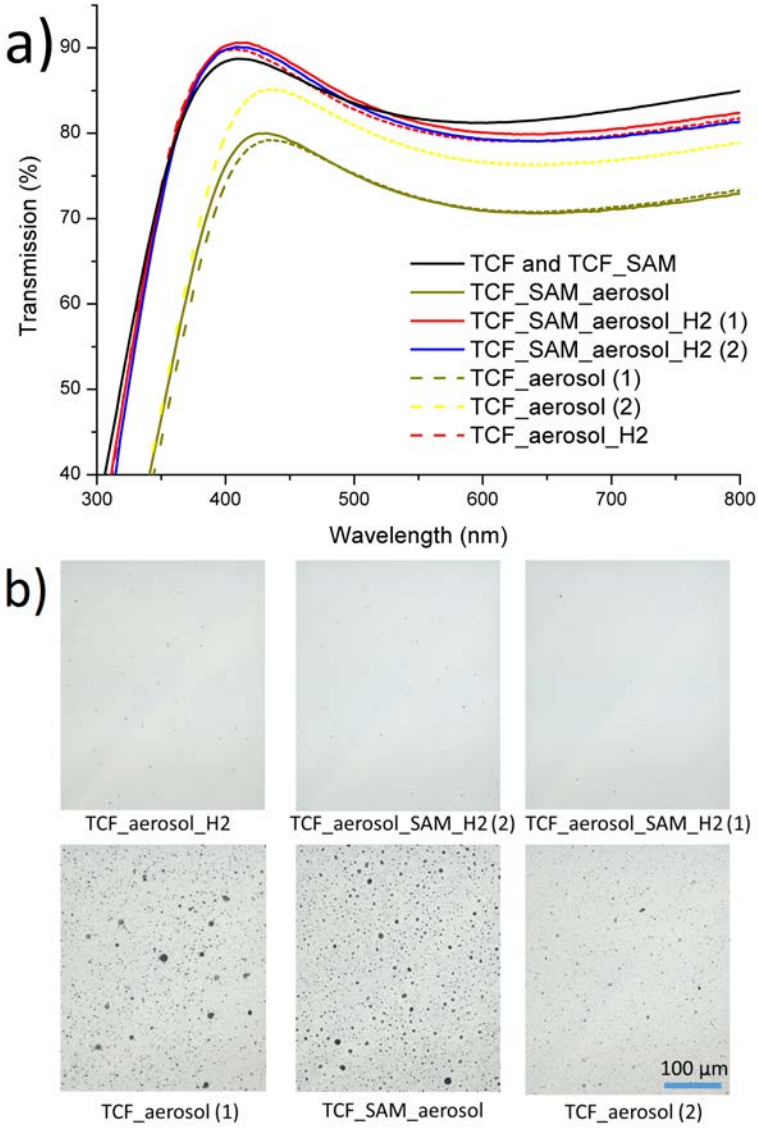

Figure 3.4: Characterization of the samples tested inside the printer. (a) Optical transmittance spectrum. (b) Light microscopy images.

cannot be seen in the transmission measurement of the samples tested inside the printer (Figure 3.4).

Comparing the ink contamination on TCF_aerosol (1) and TCF_ aerosol (2) indicates that aerosol distribution is not homogeneous in the regions where the samples were installed. They are identical samples but one has 7% of its surface area covered with ink, whereas the other has only 3% coverage. Another shortcoming of the test was the low sample size. In the lab, experiments were repeated many times, over several days. In the case of the printer test, however, one experiment takes hundreds of days and consumes one large format printer. Still, there are several conclusions that can be drawn from this experiment.

Firstly, comparing samples with/without Joule heating, a clear difference can be seen. The area covered by ink decreases from 3-7% to 0.1% upon Joule heating. The effect of SAM is not as apparent, however. For the samples without heating, the sample with SAM (TCF_SAM_aerosol) has more area covered by ink compared to the ones without SAM (TCF_aerosol (1), (2)). This was not expected because, as shown in the previous chapter, SAM increases the ink contact angle, resulting in less spreading of ink. This might be due to the very small droplet volumes. For the samples with heating, however, the samples with SAM (TCF_SAM_aerosol_ H2 (1), (2)) has less ink contamination and are more transparent than the sample without SAM (TCF_aerosol_ H2). In order to reach a conclusive result about the effect of SAM, more experiments are needed with more samples and in a setting where aerosol distribution is homogeneous.

Another unexpected behavior can be seen when the transmission behavior of the heated samples (TCF_SAM_aerosol_H2 (1), (2) and TCF_ aerosol_ H2) is compared with that of the clean samples (TCF and TCF_SAM). Within the wavelength range 350-500nm, these heated samples are even more transparent than the clean sample. This is probably due to annealing. The Joule heating action of the samples

were essentially annealing the samples for 200 days, and according to related literature, annealing increases the transparency of ITO films in the visible region [23]. Despite this, from the image analysis (Table 3.1) it can be seen that ink contamination of the heated samples is at most 0.1%, which should cause very little transmission loss.

The final conclusion is with regard to the transmission loss caused by the ink aerosol. By comparing the transmission of the clean samples (TCF and TCF_ SAM) with their contaminated counterparts (TCF_aerosol (1) and TCF_ SAM_ aerosol) it can be said that ink aerosol causes an average of 10% transmission loss in the visible region.

Chapter 4

Self-cleaning surfaces for 3D printing

4.1 Introduction

We are surrounded by particles. From subatomic particles like electrons to macroscopic particles like powder, they vary greatly in size. Macroscopic particles with sizes of between one micron and one millimeter are crucial in today's technological world. They are used in many industries, including agriculture, civil engineering, food, pharmaceuticals, energy, manufacturing and so on. As well as being crucial to today's technology, they can also be harmful. They cause air pollution, which results in both environmental and industrial health hazards, and most of the powders are explosive due to their high surface area. In addition, they are responsible for contamination to a large degree.

Powder is also used in HP 3D printers. Powders are both the building blocks of the technology, and the cause of problems related to contamination. This and the following chapter presents a solution

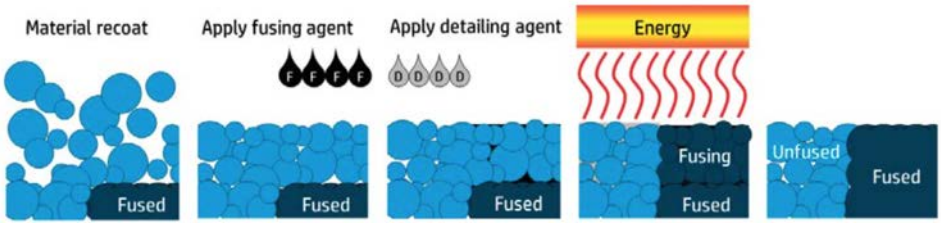

Figure 4.1: Schematic representation of HP multi jet fusion technology [3].

for powder related problems in HP 3D printers.

HP 3D printers use a technology called multi jet fusion [3]. This is a type of powder bed and inkjet head 3D printing. In multi jet fusion, firstly, a layer of powder is laid by a carriage. A second carriage passes over the powder bed applying a pair of agents, a fusing agent to define the solid layer and a detailing agent to prevent fusing of the neighboring powder. Finally, a curing lamp provides energy to catalyze the fusing agent. Figure 4.1 shows the multi jet fusion process schematically.

As with the ink aerosol contamination described in the previous chapters, a percentage of the powder flies around inside the printer, contaminating printer parts. One of these parts is the glass covering the curing lamp (represented as "energy" in Figure 4.1). This contamination causes two major problems: loss in energy transmission and glass failure due to fusing on the glass (Figure 4.2).

In this part of the thesis, we explore how we can reduce this powder contamination on printer parts, in particular on the curing lamp glass.

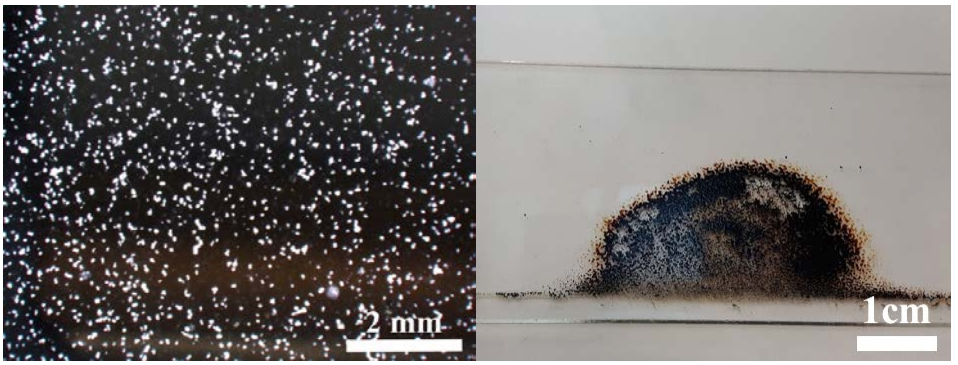

(a) (b)

Figure 4.2: (a) Powder contamination on curing lamp glass after several printing jobs (PAC 12%). (b) Glass failure due to contamination.

4.2 State of the art in powder removal

Before now, various powder/dust removal methods have been proposed [25–27], including brushing, fluid jetting, vibration, self-cleaning films and an electric curtain. Except for the electric curtain, none of these methods has proved to be useful. The electric curtain, however, has turned out to be the most feasible and widely studied/applied powder removal method available. It does not require moving parts and added mass is not significant. However, high working voltages are needed; for example, Sims et al. notes 20% cleaning at 500V and 60% cleaning at 5kV [28].

An electric curtain was first described in a NASA technical report by Tatom et al in 1967 [29]. However, their results were preliminary and they were not able to demonstrate a working example of the device. Masuda et al. developed the idea extensively laying down theoretical and experimental bases for the electric curtain, starting in 1970 [30–35]. In recent years, a team at NASA led by Dr. Carlos I.

Calle has become the greatest contributor in the development of the concept. Lunar and Martian dust is a significant problem for NASA missions. Lunar dust causes vision obscuration, false instrument readings, dust coating and contamination, seal failures and clogging during Apollo missions [36]. On the Pathfinder mission, solar cell output power decreased by 0.3% per Martian day [37]. Calle et al developed transparent electric curtains [28, 38] and tested them in environments simulating the moon [39] and Mars [40]. Testing in space has also been demonstrated [41].

Dust contamination is a serious problem, not only in space, but also on Earth. Photovoltaic systems need constant cleaning for dust contamination in order to prevent the decrease in conversion efficiency. An electric curtain has been studied among other cleaning methods to address this problem [26, 27, 42, 43].

4.3 Background

A brief introduction to particle-substrate adhesion is useful in order to understand the concept of an electric curtain. Therefore, firstly, the basics of particle adhesion will be explained and this will be followed by the fundamentals of the electric curtain concept.

4.3.1 Particle adhesion

In this section, we present the concept of adhesion, considering solid particles (1-100μm in diameter) on solid substrates in gaseous media. The interaction of particles with a solid surface is called adhesion, and autohesion is the name given to the interaction of particles with each other.

Adhesion is comprised of several different forces. First important component arises from molecular attraction. Permanent or induced

dipoles in the surface regions of two interacting bodies attract each other. This are called van der Waals interactions and they are effective over separation distances of up to 40 nm [44]. Another source of adhesion is due to capillary forces. These arise because of liquid condensation in the gaps between the particles and the surface. Thirdly, when particles are charged prior to contact, Coulomb forces might manifest between the surface and the charged particle.

The forces of adhesion are determined by external (e.g. humidity or composition of the gas medium) and internal (e.g. particle charge and shape) conditions of the particle/substrate system in question. Under specific conditions, certain components of adhesive force can override others. For example, if the particles are highly charged, Coulomb forces might govern the adhesion interaction. If, however, the contact zone is conductive or if moisture is present, charges can leak off, reducing the Coulomb forces. In fact, when the relative humidity is above 65%, capillary forces dominate over all other forces of adhesion but when the relative humidity is below 50%, capillary forces are negligible [44, 45].

If an external force is applied to a particle, detachment depends on the magnitude and direction of the applied force. Friction and adhesion both oppose removal and displacement. Friction prevents movement in a direction parallel to the surface whereas adhesion opposes displacement perpendicular to the surface. It should be noted that friction is solely caused by adhesion if there is not any external load.

4.3.2 Electric curtain

The typical electric curtain (also called an electrodynamic screen) consist of an interdigitated array of electrodes resting on a substrate. Upon the application of an AC voltage, the structure generates alternating electric fields on the surface. This field can lift and transport

charged and uncharged particles using dielectrophoretic and electrostatic forces [11].

There are two types of electric curtain: single-phase (standing waves) and poly-phase (travelling waves). Previously, it was thought that travelling wave fields were the only way to transport particles, and that standing wave fields could only levitate but not transport the particles. Recently, however, it has been shown both theoretically [4,11] and experimentally [46] that single-phase electrics curtain can transport particles. In this thesis, we have focused on single-phase electric curtains and, indeed, have shown net transport of particles.

There are two transport modes for particles excited by a single-phase electric curtain: a surfing mode and a hopping mode [11]. In the surfing mode, particles roll along the surface in a single direction. For this, electrode AC oscillation should change sign just as the particle gets to the neighboring electrode pair so that it can experience a force in a single direction (Figure 4.3). In the hopping mode, the particle receives a vertical push when it is on top of the electrode. Hopping height and length can exceed several multiples of the electrode period.

Atten et al. noted that when the operation voltage of the electric curtain is higher than the ionization voltage, dielectric barrier discharge (DBD) occurs, causing uncharged and weakly charged particles to acquire more charge. This, in turn, improves the cleaning efficiency of the electric curtain [46].

4.4 Methods

4.4.1 Design and fabrication

As previously stated, for this work, we have chosen a single-phase electric curtain. The main parameters for an electric curtain are electrode width (D) and period (L), but other parameters to consider are

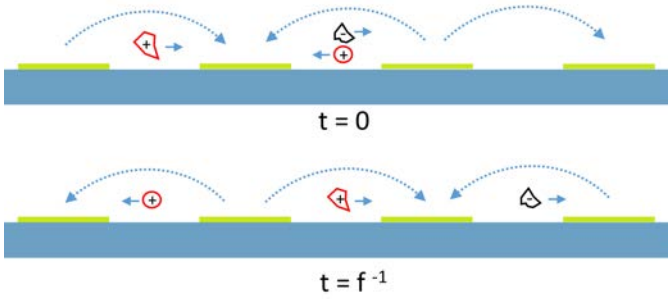

Figure 4.3: A simple schematic showing the surfing mode motion of positively and negatively charged particles on an electric curtain. Dotted lines represent the electric field, small solid arrows represent direction of particle motion, and f represents the frequency of AC oscillation.

electrode material and thickness. We used an electric curtain design with D=0.5mm and L=1mm. In order to have a transparent electric curtain, we used a 100nm thick ITO as the electrode material. This structure was fabricated on a borosilicate 3.3 substrate, which is the exact glass used in HP multi jet fusion 3D printers to cover the curing lamp. It was cut to 35x35mm pieces using a dicer and cleaned using acetone and ethanol in an ultrasonic bath. A photoresist (AZ5214E) layer was spin coated. The electrode pattern was written onto the photoresist by exposing it with the laser writer (Microtech LW405B). Later, with development (AZ726 MIF), patterns were revealed. The electrode material was deposited using sputtering (AJA International ATC Orion 8 HV), and, finally, a lift-off in acetone revealed the electric curtain structure. The electric curtain design and fabrication can be seen in Figure 4.4.

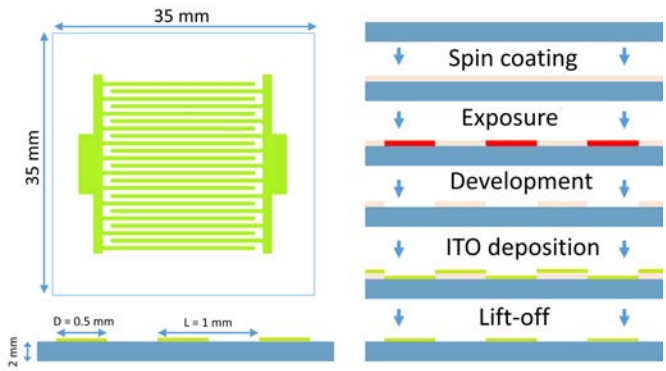

Figure 4.4: Design and fabrication of the electric curtain. Top and cross section views are given on the left hand side. A schematic of the fabrication is given on the right hand side.

4.4.2 Particle deposition

The powder used for generating contamination was polyamide 12 (also known as nylon 12) with a size distribution between 20 and 80 μm. As with the substrate, this is the type of powder used in HP MJF 3D printers. A spray setup was built the for powder deposition (Figure 4.5). This utilized a powder blower (Model 119, DeVilbiss) which was connected to a pressure controller and a purge valve. The pressure controller sets the pressure going into the powder blower and the purge valve sets the blowing time. During the experiments initial powder contamination was kept between 20 and 40% PAC, and humidity during deposition and signal application was kept below 50% RH in order to prevent capillary forces coming into play.

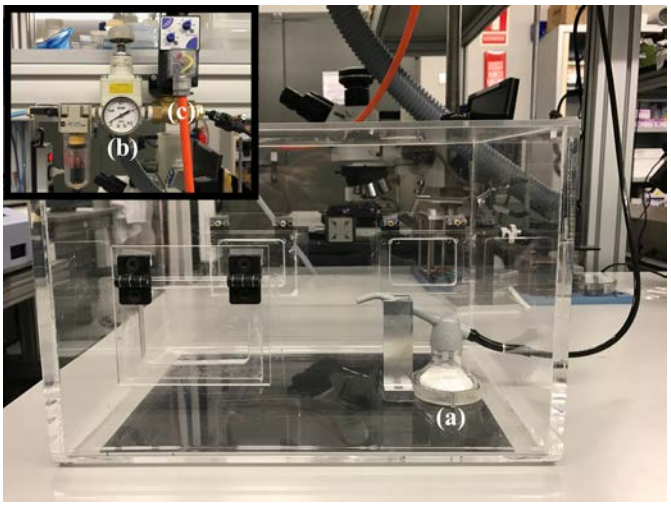

Figure 4.5: Image of the powder deposition setup showing (a) powder blower, (b) pressure controller, and (c) purge valve.

4.4.3 Signal application

A digital waveform generator (BK Precision 4052) was used to generate the AC signal. It was connected to a high-voltage amplifier (Trek 20/20C) which can amplify the signal by a factor of 2000. Applied voltage refers to the amplitude of the signal, unless otherwise stated. An oscilloscope (YOKOGAWA DML2024) was used to monitor the signal. For safety reasons, the signal application to the electric curtain was conducted inside an insulating box, which shuts off the amplifier when the lid is open. This setup is shown in Figure 4.6.

4.4.4 Characterization

A USB microscope (XCSOURCE USB 20X-800X) was placed into the electric curtain setup for taking in situ images and videos of the

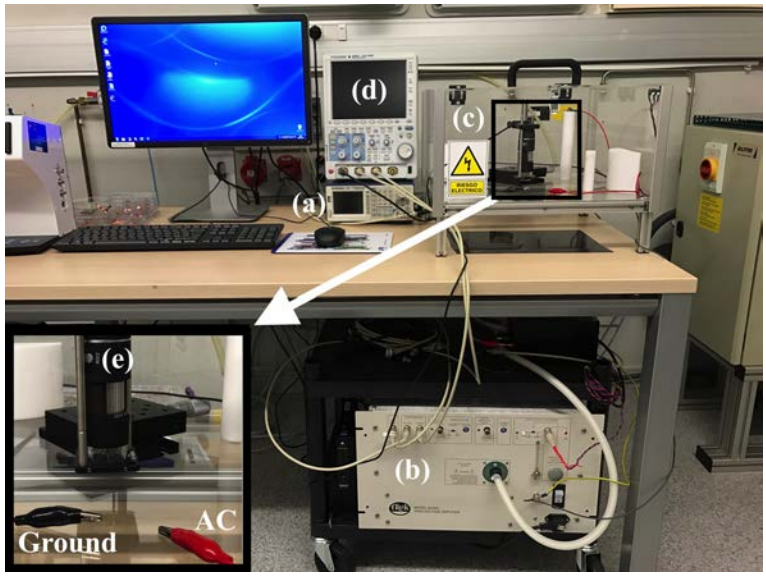

Figure 4.6: Image of the electric curtain setup showing (a) waveform generator, (b) high voltage amplifier, (c) insulating box, and (d) oscilloscope. Inset shows (e) USB microscope and terminals.

experiment (Figure 4.6 (e)). Later, the images were analyzed using an image processing software (ImageJ) to calculate the percent area covered (PAC) by powder. Using the PAC values before and after the electric curtain application, the cleaning factor (CF) was determined. The CF is the figure of merit for the electric curtain and it can be described as the ratio of removed powder to initial powder content (Eq 4.1). For any given applied voltage, the CF value of the electric curtain was calculated on 3 identical samples and the experiment was repeated 3 times for each sample.

$$Cleaning factor(\%) = \frac{Initial powder - Remaining powder}{Initial powder} * 100 \tag{4.1}$$

4.5 Results and Discussion

Before testing the electric curtain (EC) performance, transmission of the structure was measured and compared with the bare substrate (Figure 4.7). It can be seen that the drop in transmission due to the electrodes is around 7% at wavelengths below 1500nm, increasing to 20% in the IR as the ITO absorbs the IR.

To assess the performance of the device, a signal was applied suddenly at various voltages and the cleaning factor for each experiment was calculated. This was carried out for three identical samples, and repeated three times for each. The cleaning factor (CF) vs. applied voltage (V) curve for D=0.5mm and L=1mm with a 100nm ITO is given in Figure 4.8. Light microscopy images are given at 3 different voltages (Figure 4.9).

At first sight, from Figures 4.8-4.9, it can be deduced that the proposed structure can mitigate nylon 12 on borosilicate 3.3. Generally

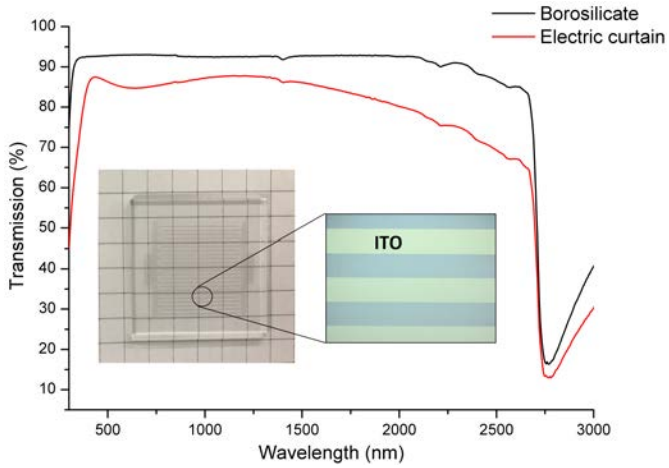

Figure 4.7: Transmission behavior of the electric curtain compared to the bare substrate. Inset shows the image of a fabricated sample.

speaking, it can be said that as the voltage increases, the cleaning increases. However there are different regions and, initially, (up to 100 V) no particle movement was observed. This is because the electrical force on the particles was less than the adhesion force.

Between 100 and 200 V, individual particle movements were observed, but there was still no bulk movement. There might be several reasons for this individual behavior. Firstly, some particles might have a higher charges than others, meaning that the electrical force could be higher, helping them to overcome the adhesion force below 200V. Secondly, particles are not perfect spheres, but, rather, they are irregularly shaped objects. This creates a unique contact geometry between each particle and the substrate. In addition, particle sizes vary. For these reasons, the adhesion force is not equal for all particles and, therefore, individual particles with lower adhesion might readily move below 200V.

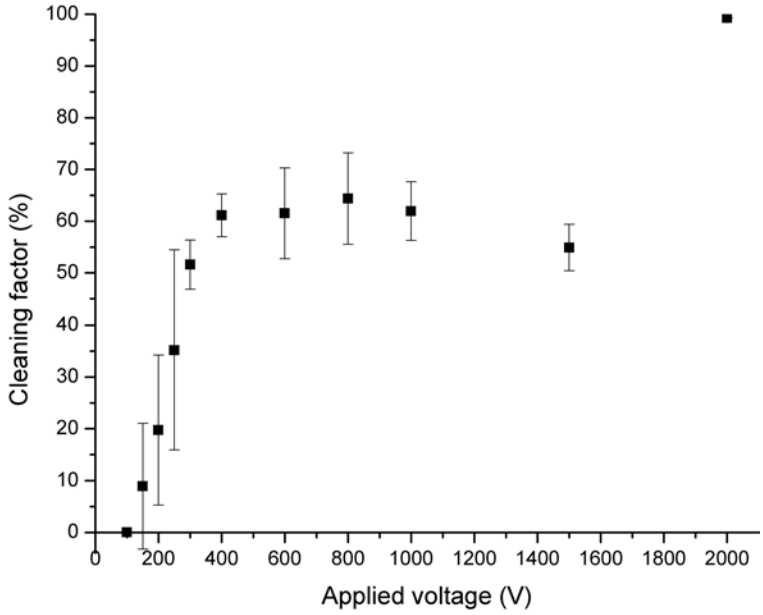

Figure 4.8: Cleaning factor (CF) vs. applied voltage (V) for a 100nm ITO electric curtain with D=0.5mm and L=1mm. Error bars represent the standard deviation. For the CF at 2000V, the standard deviation is smaller than the square itself.

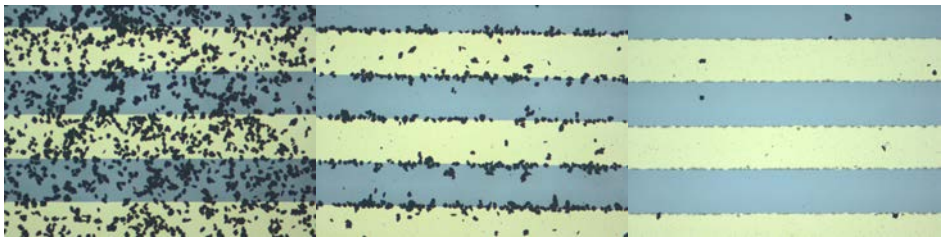

(a) (b) (c)

Figure 4.9: Light microscopy images of the samples at three different voltages (a) 0 V (b) 600 V and (c) 2000 V. Yellow stripes are the electrodes and gray is the substrate.

(a) (b) (c)

Figure 4.10: Edges of the EC after cleaning.

Above 200V, bulk movement begins and almost all particles start moving. This means that the electrical force is larger than the adhesion force for most of the particles. The majority of these particles move parallel to the surface in the direction perpendicular to the electrodes, and move out of the region covered by the electrodes. They stop right after the last electrode, which can be confirmed by looking at the edges (Figure 4.10a and 4.10b). Powder movement in the direction parallel to the electrode length is insignificant. The amount of powder in Figure4.10c is similar to the initial powder contamination.

As the voltage increases above 200V, the cleaning factor increases further because of a greater force on the particles. Hence, one would expect this to go on until almost all of the particles are removed, but, rather, the cleaning effect saturates after 400V, with a 60% cleaning factor.

Between 600 and 1500V, the cleaning factor remains more or less the same. The possible reason for this can be deduced by looking at Figure 4.9b. The remaining particles are not randomly distributed, but, rather, most of them are located at the electrode edges as if they are 'stuck' there. The reason behind this has been explained by Sun et al. [4] by plotting forces perpendicular to the electrode with respect to position (Figure 4.11). The positions where the forces are zero or negative are indicated as traps. This means that if a particle is initially at a trap, it will not move. Also, if a particle passing over a trap does not have enough inertia, it will get stuck there. Edge traps are more effective due to negative forces there, meaning particles are drawn to the traps, whereas the trap at the center of the electrode is only a point of zero force.

Above 1500V, sparks were observed due to dielectric barrier discharge (DBD). These sparks were seen locally at some regions of the electrodes, extending to the whole surface of the electric curtain at around 2000V. At this voltage, sparks were observed over the whole electrode structure, removing almost all the powder. This has been observed previously, and the reason why DBD improves cleaning is explained before in section 4.3.2.

4.6 Conclusions

In this chapter, a structure capable of reducing powder contamination has been demonstrated. The powder and the substrate to be cleaned were the same materials used in HP MJF 3D printers. It has been

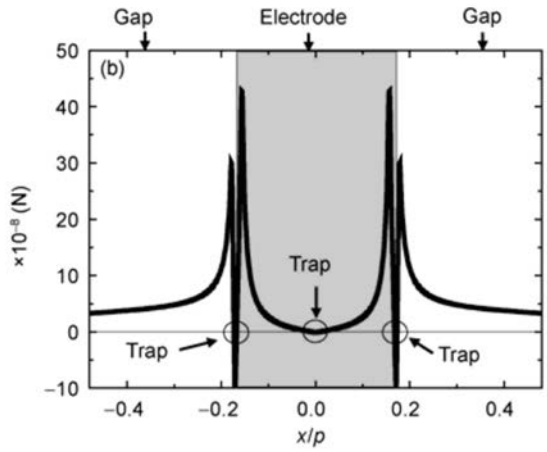

Figure 4.11: Force vs. position showing places where forces are zero or negative [4].

shown that cleaning performance depends on the applied voltage. At 600V, for example, 60% cleaning is observed, whereas above 1500V, sparks due to DBD occur and the cleaning factor increases to 99%.

Edge traps were identified as the phenomena preventing complete cleaning below 1500V. Most of the particles remaining after cleaning were observed at the edge traps. The next chapter describes a novel structure to decrease/eliminate these edge traps.

Chapter 5

Double layer electric curtain

5.1 Introduction

In the previous chapter, a transparent surface capable of mitigating powder was demonstrated. This surface was comprised of an electric curtain. It was shown that 60% of the initial contamination could be removed. This could be extended up to 99% when the working voltage surpasses the DBD. After cleaning, most of the remaining particles were observed at the edges of the electrodes. This is due to the trap states shown in Figure 4.11, which are caused by the high concentration of the electric field at the electrode edges. If these trap states can be eliminated, i.e. if the electric field at the electrode edges can be reduced, one could expect cleaning to improve.

We propose a double layer electric curtain to address this issue. Figure 5.1 shows the cross-section of the double layer electric curtain, together with a light microscopy image of a fabricated sample (top view). The top layer geometry was the same as used previously, i.e. D=0.5mm and L=1mm, and the geometry of the bottom layer was chosen to be D=0.6mm and L=1mm. For the electric field lines to

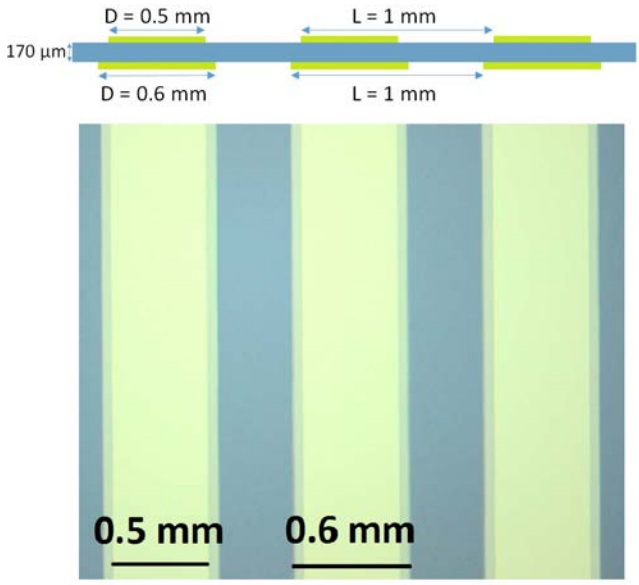

Figure 5.1: Double layer electric curtain. Top scheme shows the cross-section and below is the top view of a fabricated sample.

penetrate, a thinner substrate was needed. Therefore 170 μm thick coverslips (Menzel - D 263 M borosilicate glass) were used as the substrate.

With this structure, it was anticipated that the electric field at the electrode edges could be modified.

5.2 Methods

Fabrication methods were identical to the ones described for the single layer electric curtain, the only difference being the need for alignment of the top and bottom layer electric curtains. This was achieved using

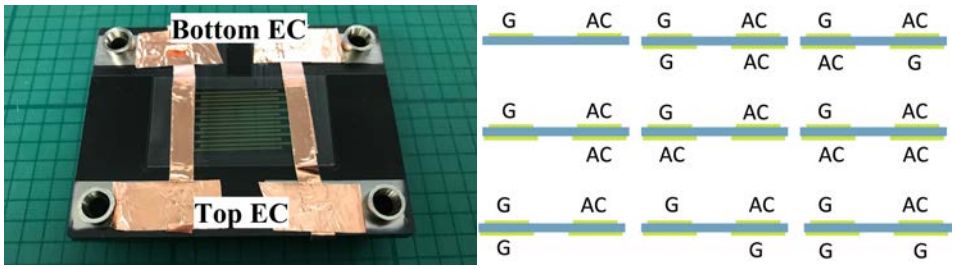

(a) (b)

Figure 5.2: (a) Double layer EC with 4 terminals. Terminal pairs connected to the top and bottom EC's are indicated on the image (b) Combinations of potentials applied to the double layer EC. 'G' refers to the electrode connected to the ground and 'AC' refers to the electrode with the voltage alternating between +V and -V.

the laser writer software. The same powder deposition and signal application systems were used to test the samples.

The structure was tested as follows: Terminals for the top electric curtain were held constant, but for the bottom electric curtain, various combinations were tested. Figure 5.2 shows an example of the double layer EC device with its 4 terminals and the combination of potentials applied to these terminals.

For characterization purposes, an electric field simulation and an electric curtain test were conducted for each case shown in Figure 5.2. For the simulations COMSOL, a commercial finite element analysis software was used.

As described in the previous chapter, the cleaning factor (CF) is the performance figure of merit for an electric curtain. On a single layer electric curtain, both terminals (i.e. ground and AC) have identical electric field distributions, causing the amount of particles sticking at the edges to be identical. On the double layer electric curtain,

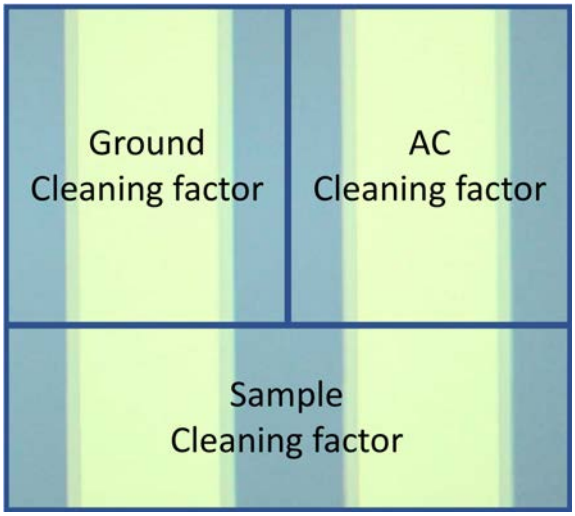

Figure 5.3: Areas used to calculate CFs.

however, depending on the configuration, different electric fields can be observed for G and AC electrodes on the same sample. This causes localized variations of the cleaning factor. Therefore, three different cleaning factor values are given for these samples: firstly, for the area around the ground electrode, secondly, for the area around the AC electrode, and thirdly, for the entire sample. Figure 5.3 shows the areas used to calculate these three cleaning factors.

5.3 Results and discussion

For each case represented in Figure 5.2, the electric field simulation, the image of the sample after the electric curtain (EC) application, and the related cleaning factor values are given in Figure 5.4.

At first glance, one can see that the bottom electric curtain can indeed change the electric field at the edges of the top electric curtain.

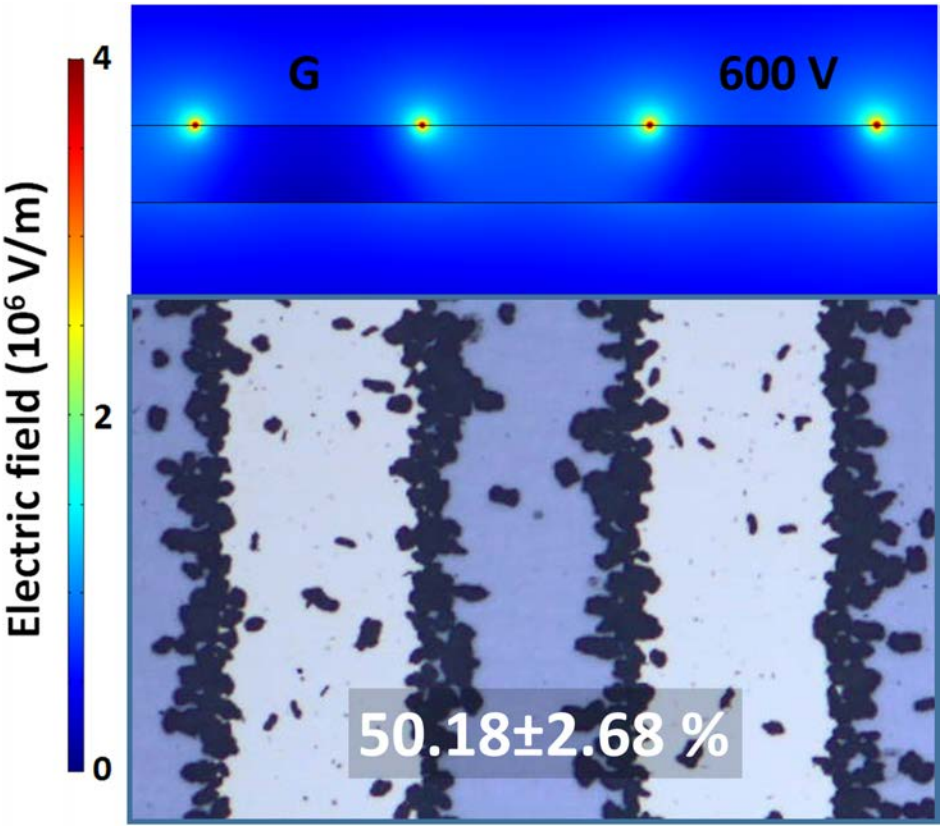

Figure 5.4: (a) E-field simulation and CF for the single layer EC.

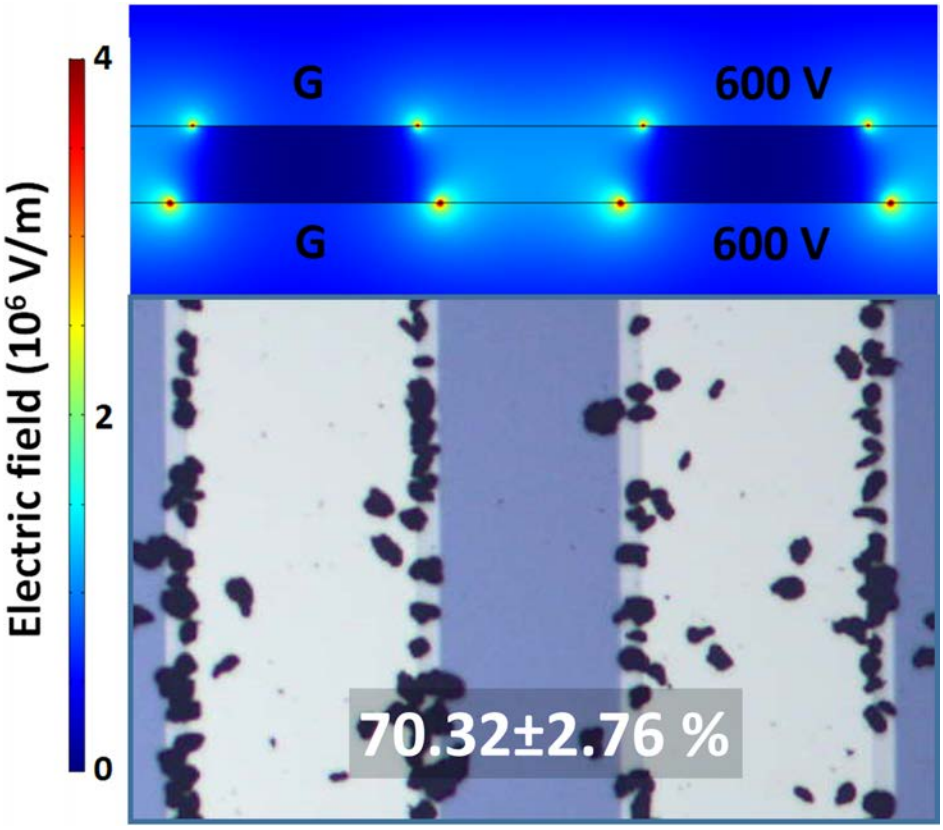

Figure 5.4: (b) E-field simulation and CF for the double layer EC.

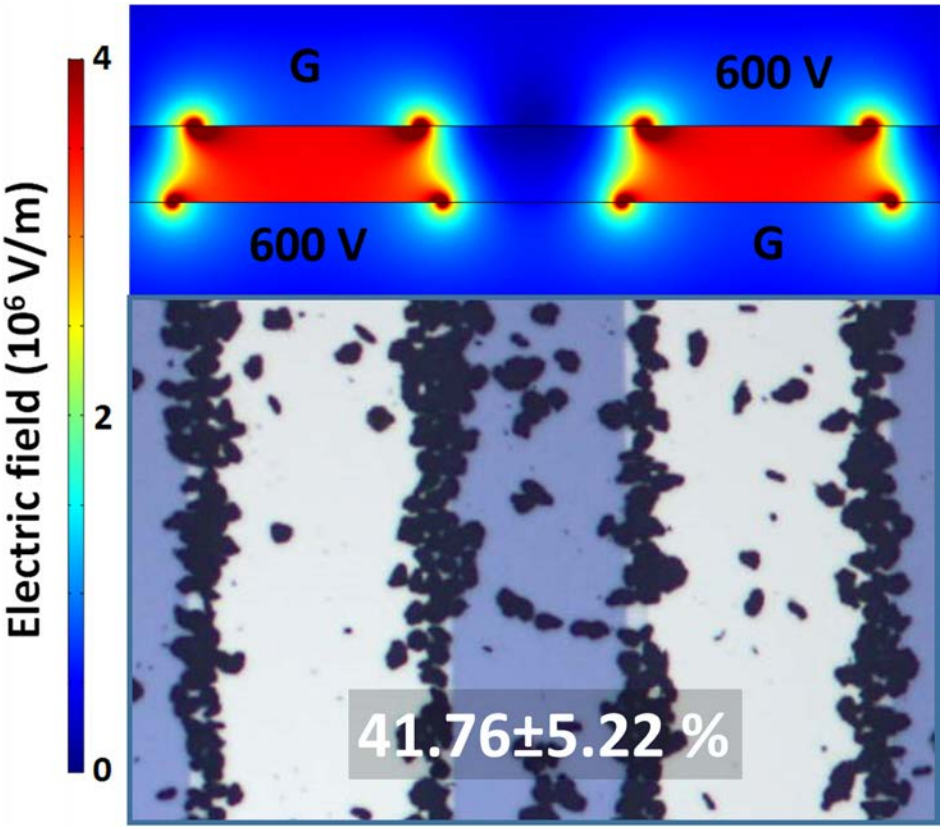

Figure 5.4: (c) E-field simulation and CF for the double layer EC structure, where opposite electrodes are on top of each other.

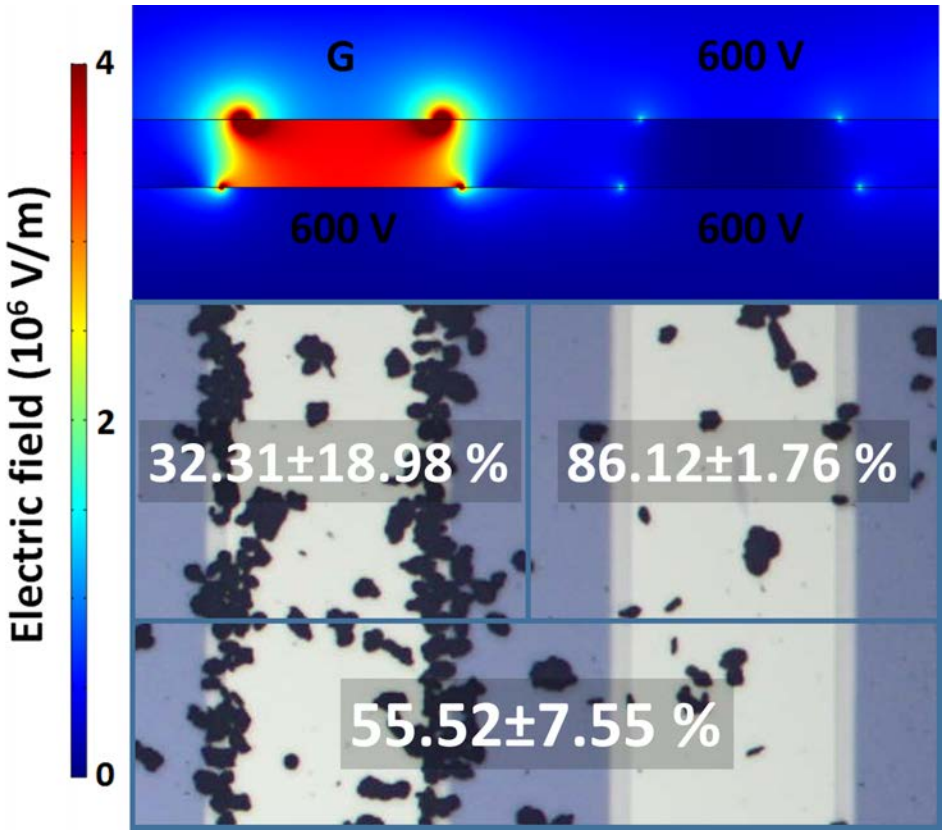

Figure 5.4: (d) E-field simulation and CF for the double layer EC, where all bottom electrodes are connected to AC.

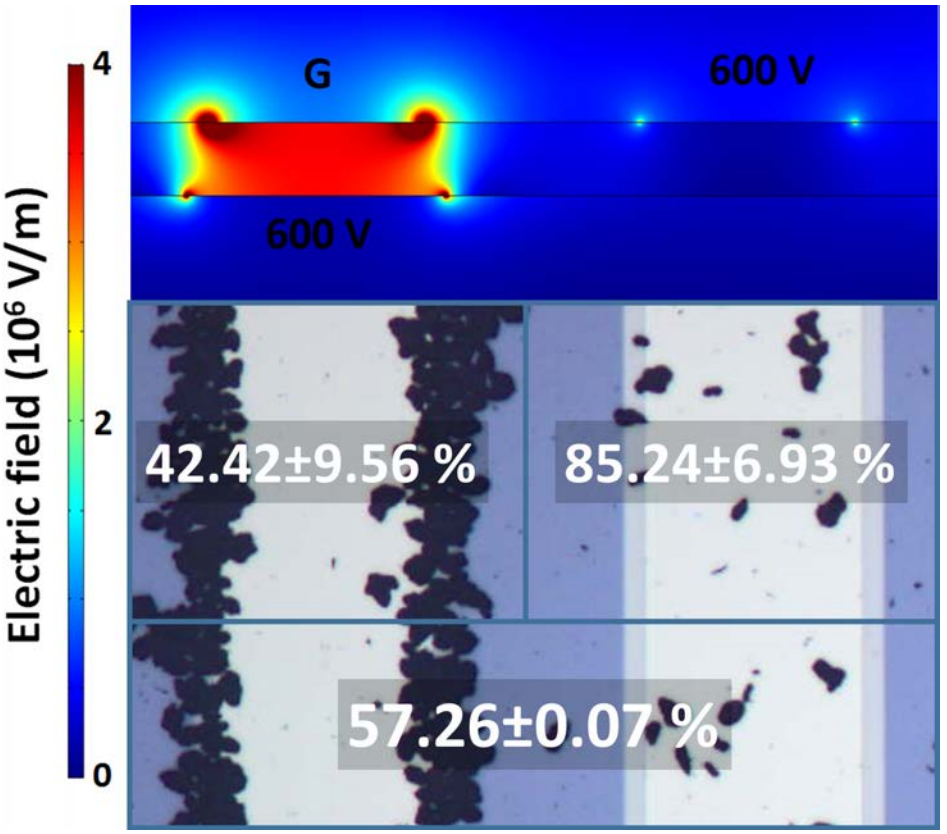

Figure 5.4: (e) E-field simulation and CF for the double layer EC, where AC is placed under G electrode.

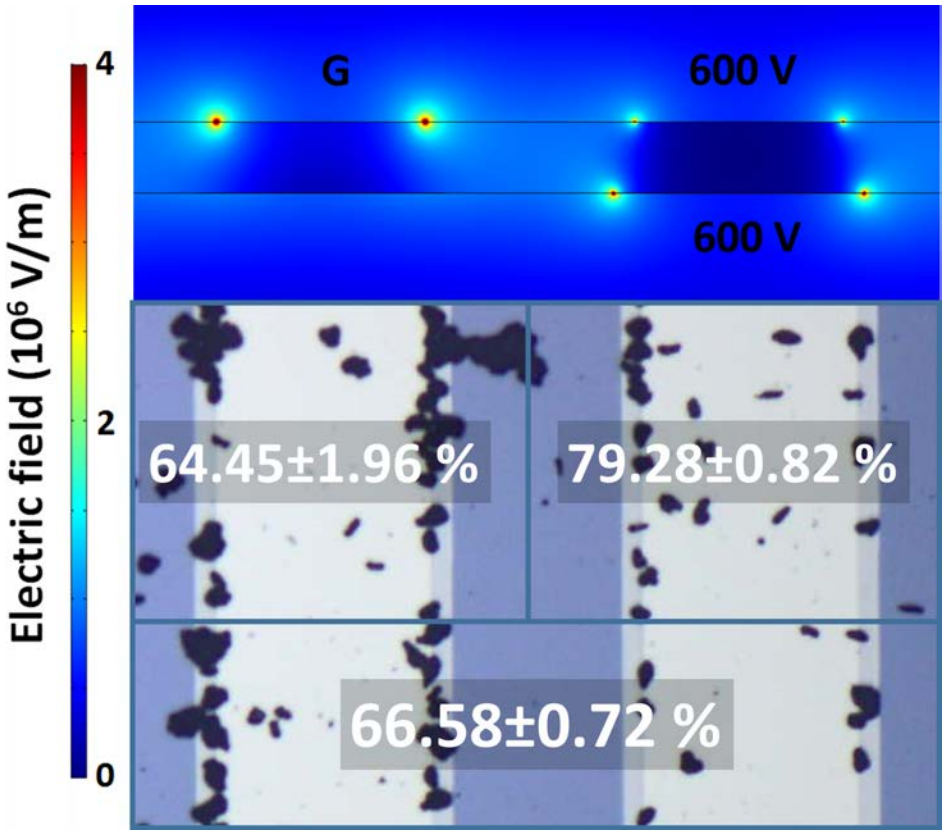

Figure 5.4: (f)E-field simulation and CF for the double layer EC, where AC is placed under AC electrode.

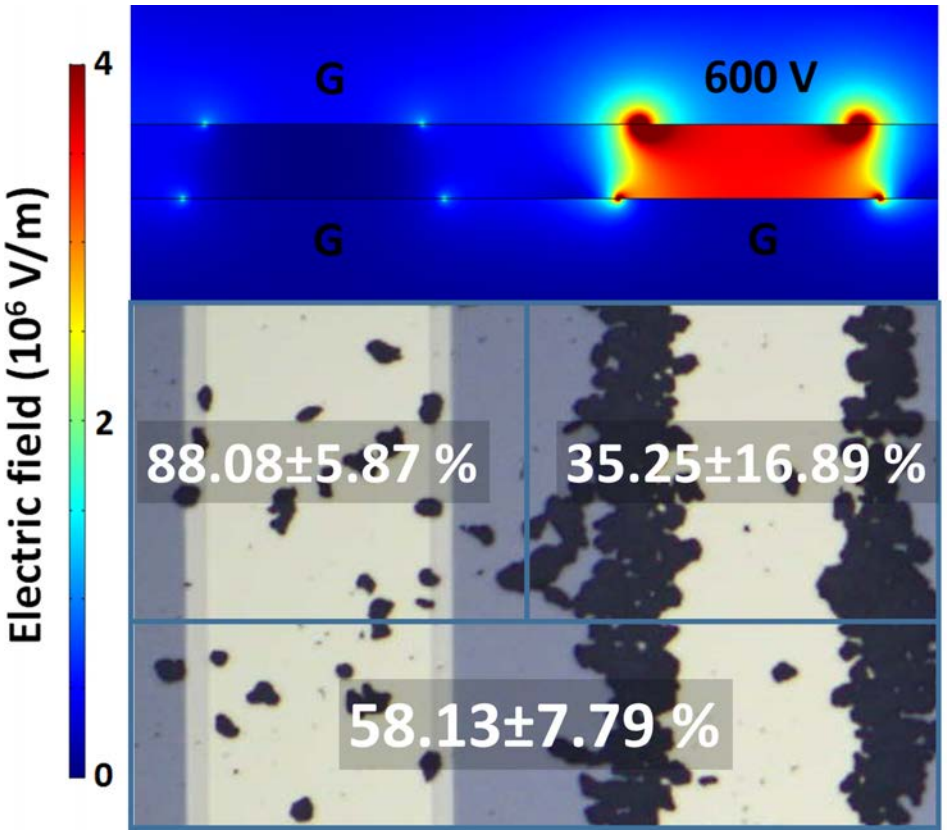

Figure 5.4: (g) E-field simulation and CF for the double layer EC, where all bottom electrodes are connected to G.

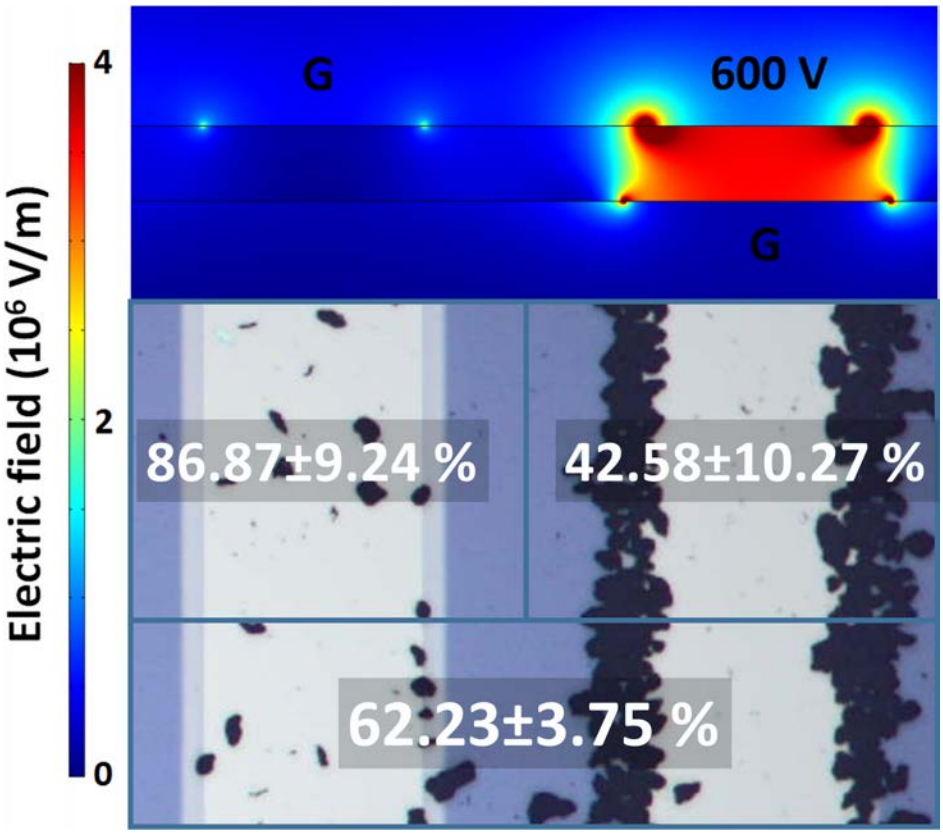

Figure 5.4: (h) E-field simulation and CF for the double layer EC, where G is placed under AC electrode.

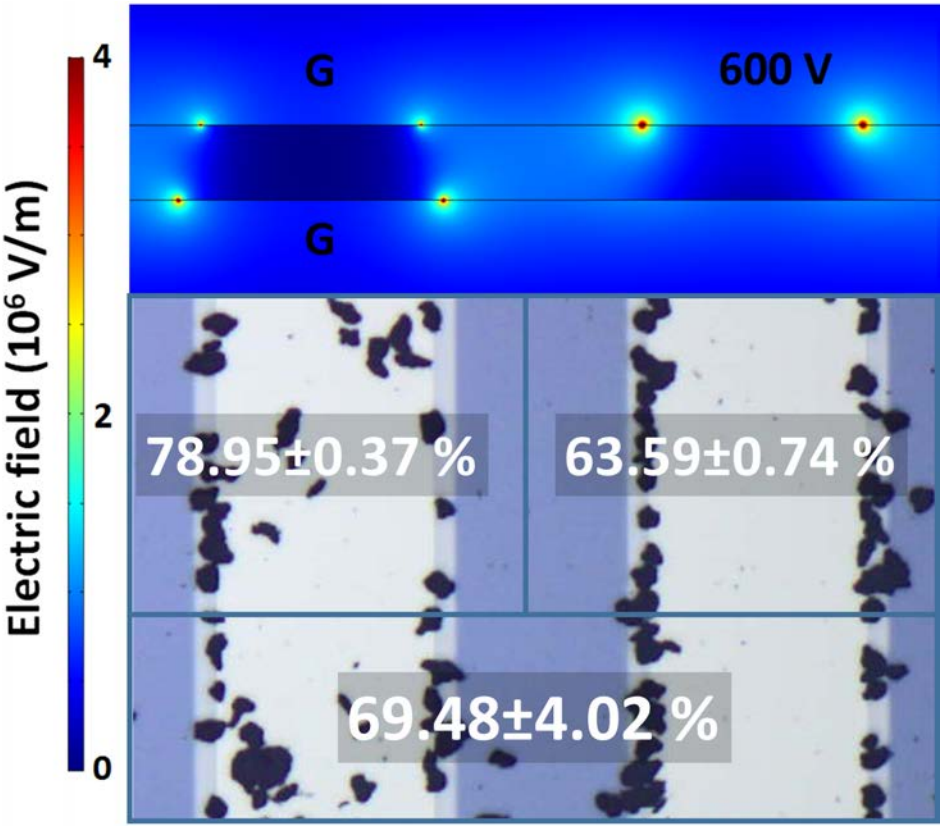

Figure 5.4: (i) E-field simulation and CF for the double layer EC, where G is placed under G electrode.

Depending on the configuration, it either lowers the electric field or it increases it, or it does both at the same time.

It can be said that the simulations and experiments are in good agreement with each other. As the electric field concentration at the edges of the electrodes decreases, particle sticking at the edges decrease as well. The cleaning factor for the areas around the individual electrodes was used as a measure for the particles sticking at the edges. The higher the cleaning factor for an electrode, the lower the number of particles sticking to that electrode.

Compared to the single layer electric curtain (Figure 5.4a) there is one configuration with a lower electric field concentration at the edges (Figure 5.4b), and one with a higher electric field concentration (Figure 5.4c). In addition, there are several configurations where one electrode has lower traps and the other has higher traps on the same sample, compared to the single layer electric curtain (Figures 5.4d-i). Among these, some configurations deviate significantly from the single layer, where traps are completely eliminated in one electrode and very strong on the opposing electrode (Figures 5.4d,e,g,h), whilst, for the others, the deviation is smaller (Figures 5.4f,i).

In conclusion, a structure that can reduce electric field concentration at the electrode edges, hence the trapping effects, has been introduced (Figure 5.4b). The idea behind decreasing the edge traps was to improve cleaning. Indeed, it has been shown that this structure increases the cleaning factor from 50% for the single layer electric curtain to 70% for the double layer. In addition to this, other combinations were demonstrated, where in one electrode, traps are almost completely eliminated but the opposing electrode has more traps. With these structures, local cleaning factors rise above 85% around the electrode where traps are eliminated (Figures 5.4d,e,g,h).

Chapter 6

Conclusions

Self-cleaning surfaces are promising for a wide range of applications with many industries that can benefit from these technologies. This thesis has demonstrated novel self-cleaning surfaces for printing devices.

In particular, a surface combining Joule heating and hydrophobicity to be used against ink aerosol contamination in inkjet printers and another surface capable of reducing powder contamination occurring inside 3D printers have been proposed and developed for the first time to our knowledge.

In Chapter 2, we investigated the self-cleaning effect of transparent surfaces covered with transparent conductive films (TCFs) and a self-assembled monolayer (SAM) against ink aerosol contamination that occurs in printers. Although Joule heating and hydrophobicity reduced ink aerosol contamination individually, the optimal results were seen when these two methods were combined. Without hydrophobicity or Joule heating, the transmittance loss was as high as 20%, the average loss being around 10%. On the other hand, when the samples were treated with both hydrophobicity and Joule heating the transmittance loss dropped significantly to 1.5%. In addition, this treatment

reduced the percentage of the area covered by ink from 45.62±6.15 % to 1.71±0.25%. The results obtained from the glass substrates were extended to the "real" plastic windows used in the calibration sensors of inkjet printers, which demonstrates the viability of the method in the printing industry.

In the next chapter, Chapter 3, these surfaces were tested inside a large format inkjet printer. The results revealed that these surfaces are indeed able to reduce ink aerosol contamination generated inside an actual printer. However, some differences were noted. The effect of Joule heating on the cleaning performance was obvious and it seemed to be the main mechanism for cleaning. On the other hand, regarding the effect of SAM, no conclusive result could be reached due to low sample size and non-homogeneity of the ink aerosol contamination.

In chapter 4, a structure consisting of co-planar transparent electrodes capable of reducing the powder contamination was demonstrated. While 60% cleaning was observed at 600V, the cleaning factor increased to 99% above 1500V due to sparks that occur as a result of dielectric barrier discharge (DBD). Edge traps caused by the concentration of the electric field at the electrode edges were identified as the limiting factor for cleaning to reach above 60%. To address this problem, a novel structure was proposed and described in Chapter 5.

This new structure, named double layer electric curtain, consisted of multilayer co-planar transparent electrodes and allowed reducing electric field concentration at the electrode edges, hence the trapping effects. This in turn leads to a much higher level of cleaning and particle removal. For the specific conditions (material, voltage etc.) reported in the thesis, this method increased the cleaning factor from 50% for the single layer curtain to 70% for the double layer electric curtain. In some structures local cleaning factors going above 85% were observed due to almost complete elimination of the trap states.

Outlook Though the results of the thesis are very promising and as such being protected by patents and trademark secret in some cases, there is still further room for significant improvements to the cleaning performances of the surfaces presented.

Only flat hydrophobic surfaces were studied for ink repellent surfaces. However, it is widely known that surface roughness combined with hydrophobic coatings would reveal super-hydrophobic surfaces, increasing water contact angles much above 120°. This might improve the cleaning performance. However, this is not a straightforward process as cleaning depends on the fact that the droplet stays in the Cassie-Baxter state (the droplet hanging on the structures). But on active surfaces, Cassie-Baxter to Wenzel (the droplet filling in the structures) transition is likely to occur which would hinder cleaning. Nevertheless, specific topographical structures could be designed to prevent this transition.

For the powder cleaning surfaces, focus could be given to the study of powder-substrate adhesion, not only displacement. Lowering adhesion might result in two positive outcomes. Firstly, it might prevent powder from sticking to the surface. Secondly, it might lower the working voltages for the electric curtain because, for a fixed electrode design and signal frequency and shape, the working voltage depends on the adhesive force between the powder and the substrate.

Bibliography

[1] n-tech research, "Markets for Self-Cleaning Coating and Surfaces: 2015 to 2022," tech. rep., 2015.

[2] B. Bhushan and H. Liu, "Self-Assembled Monolayers for Controlling Adhesion, Friction and Wear," in *Nanotribology and Nanomechanics*, pp. 885–928, Berlin/Heidelberg: Springer-Verlag, 2005.

[3] "HP Multi Jet Fusion technology," Tech. Rep. 4AA4-5472ENW, http://www8.hp.com/h20195/v2/GetPDF.aspx/4AA4-5472EEW.pdf, 2014.

[4] Q. X. Sun, N. N. Yang, X. B. Cai, and G. K. Hu, "Mechanism of dust removal by a standing wave electric curtain," *Science China: Physics, Mechanics and Astronomy*, vol. 55, no. 6, pp. 1018–1025, 2012.

[5] W. Barthlott and C. Neinhuis, "Purity of the sacred lotus, or escape from contamination in biological surfaces," *Planta*, vol. 202, pp. 1–8, 4 1997.

[6] C. Neinhuis, "Characterization and Distribution of Water-repellent, Self-cleaning Plant Surfaces," *Annals of Botany*, vol. 79, pp. 667–677, 6 1997.

[7] W. Barthlott, "Self-cleaning surfaces of objects and process for producing same," no. US6660363 B1, 1995.

[8] C. D. Bandara, S. Singh, I. O. Afara, A. Wolff, T. Tesfamichael, K. Ostrikov, and A. Oloyede, "Bactericidal Effects of Natural Nanotopography of Dragonfly Wing on Escherichia coli," *ACS Applied Materials & Interfaces*, vol. 9, pp. 6746–6760, 3 2017.

[9] J. Lemire, J. Harrison, and R. Turner, "Antimicrobial activity of metals: mechanisms, molecular targets and applications," *Nature Reviews Microbiology*, 2013.

[10] S. Kiruthika, R. Gupta, G. U. Kulkarni, J. Zhao, S. Garner, P. Cimo, Z. Barcikowski, A. Mignerey, L. Hu, Y. H. Lee, and J.-U. Park, "Large area defrosting windows based on electrothermal heating of highly conducting and transmitting Ag wire mesh," *RSC Adv.*, vol. 4, pp. 49745–49751, 10 2014.

[11] G. Liu and J. S. Marshall, "Particle transport by standing waves on an electric curtain," *Journal of Electrostatics*, vol. 68, no. 4, pp. 289–298, 2010.

[12] P. Calvert, "Inkjet Printing for Materials and Devices," *Chemical Materials*, vol. 13, pp. 3299–3305, 2001.

[13] G. Cummins and M. P. Desmulliez, "Inkjet printing of conductive materials: a review," *Circuit World*, vol. 38, no. 4, pp. 193–213, 2012.

[14] J. T. Delaney, P. J. Smith, and U. S. Schubert, "Inkjet printing of proteins," *Soft Matter*, vol. 5, no. 24, p. 4866, 2009.

[15] M. Singh, H. M. Haverinen, P. Dhagat, and G. E. Jabbour, "Inkjet printing-process and its applications," *Advanced Materials*, vol. 22, no. 6, pp. 673–685, 2010.

[16] T. Xu, J. Jin, C. Gregory, J. J. Hickman, and T. Boland, "Inkjet printing of viable mammalian cells," *Biomaterials*, vol. 26, no. 1, pp. 93–99, 2005.

[17] S. D. Hoath, *Fundamentals of Inkjet Printing: The Science of Inkjet and Droplets*. Wiley-VCH, 2016.

[18] C. L. Holstun and S. D. Asakawa, "Selection of printing conditions to reduce ink aerosol," no. US7066564 B2, 2006.

[19] M. Boleda, R. R. Giles, and P. D. Gast, "Ink aerosol control for large format printer," no. US6203152 B1, 2001.

[20] P. Ragesh, V. Anand Ganesh, S. V. Nair, and A. S. Nair, "A review on 'self-cleaning and multifunctional materials'," *Journal of Materials Chemistry A*, vol. 2, p. 14773, 6 2014.

[21] H. Lemire, K. Peterson, M. Breslau, K. Singer, I. Martin, and R. H. French, "Degradation of Transparent Conductive Oxides, and the Beneficial Role of Interfacial Layers," *MRS Proceedings*, vol. 1537, no. mrss13-1537, 2013.

[22] N. J. Shirtcliffe, G. McHale, S. Atherton, and M. I. Newton, "An introduction to superhydrophobicity.," *Advances in colloid and interface science*, vol. 161, pp. 124–38, 12 2010.

[23] S. Song, T. Yang, J. Liu, Y. Xin, Y. Li, and S. Han, "Rapid thermal annealing of ITO films," *Applied Surface Science*, vol. 257, no. 16, pp. 7061–7064, 2011.

[24] R. N. Udey, a. D. Jones, and G. R. Farquar, "Aerosol and Microparticle Generation Using a Commercial Inkjet Printer," *Aerosol Science and Technology*, vol. 47, no. 4, pp. 361–372, 2013.

[25] G. Landis, "Mars dust removal technology," *IECEC-97 Proceedings of the Thirty-Second Intersociety Energy Conversion Engineering Conference (Cat. No.97CH6203)*, vol. 1, pp. 764–767, 1997.

[26] G. He, C. Zhou, and Z. Li, "Review of self-cleaning method for solar cell array," *Procedia Engineering*, vol. 16, pp. 640–645, 2011.

[27] A. Alshehri, B. Parrott, A. Outa, A. Amer, F. Abdellatif, H. Trigui, P. Carrasco, S. Patel, and I. Taie, "Dust mitigation in the desert: Cleaning mechanisms for solar panels in arid regions," *2014 Saudi Arabia Smart Grid Conference, SASG 2014*, pp. 1–6, 2015.

[28] R. A. Sims, A. S. Biris, J. D. Wilson, C. U. Yurteri, M. K. Mazumder, C. I. Calle, and C. R. Buhler, "Development of a transparent self-cleaning dust shield for solar panels," *Proceedings ESA-IEEE joint meeting on electrostatics*, no. 1, pp. 814–821, 2003.

[29] F. B. Tatom, V. Srepel, R. D. Johnson, N. A. Contaxes, J. G. Adams, H. Seaman, and B. L. Cline, "Lunar dust degradation effects and removal/prevention concepts," Tech. Rep. TR-792-7-207A, Northrop Space Laboratories, 1967.

[30] S. Masuda, K. Fujibayashi, and K. Ishida, "Electrodynamic behaviour of charged aerosol particles in non-uniform alternating fields and its applications in dust control," *Staub-Reinhaltungs der Luft*, vol. 30, no. 11, pp. 449–456, 1970.

[31] S. Masuda, K. Fujibayashi, K. Ishida, and H. Inaba, "Confinement and transportation of charged aerosol clouds via electric curtain," *Electrical Engineering in Japan*, vol. 92, no. 1, pp. 43–52, 1972.

[32] S. Masuda and Y. Matsumoto, "Theoretical characteristics of standingwave electric curtains," *Electrical Engineering in Japan*, vol. 93, no. 1, 1973.

[33] S. Masuda, Y. Matsumoto, and K. Akutsu, "Characteristics of standingwave, ringtype electric curtain. experimental study," *Electrical Engineering in Japan*, vol. 93, no. 1, 1973.

[34] S. Masuda and T. Kamimura, "Approximate methods for calculating a non-uniform travelling field," *Journal of Electrostatics*, vol. 1, no. 4, pp. 351–370, 1975.

[35] S. Masuda, M. Washizu, and I. Kawabata, "Movement of blood cells in liquid by nonuniform traveling field," *IEEE Transactions on Industry Applications*, vol. 24, no. 2, pp. 217–222, 1988.

[36] J. R. Gaier, "The Effects of Lunar Dust on EVA Systems During the Apollo Missions," *Nasa/Tm-2005-213610/Rev1*, no. March, pp. 1–16, 2007.

[37] G. A. Landis and P. P. Jenkins, "Measurement of the settling rate of atmospheric dust on Mars by the MAE instrument on Mars Pathfinder," *Journal of Geophysical Research*, vol. 105, no. E1, p. 1855, 2000.

[38] C. I. Calle, J. L. Mcfall, C. R. Buhler, S. J. Snyder, and E. E. Arens, "Dust Particle Removal by Electrostatic and Dielectrophoretic Forces with Applications to NASA Exploration Missions," *ESA Annual Meeting on Electrostatics*, p. 1, 2008.

[39] C. I. Calle, C. R. Buhler, J. L. McFall, and S. J. Snyder, "Particle removal by electrostatic and dielectrophoretic forces for dust control during lunar exploration missions," *Journal of Electrostatics*, vol. 67, no. 2-3, pp. 89–92, 2009.

[40] C. I. Calle, C. R. Buhler, M. R. Johansen, M. D. Hogue, and S. J. Snyder, "Active dust control and mitigation technology for lunar and Martian exploration," *Acta Astronautica*, vol. 69, no. 11-12, pp. 1082–1088, 2011.

[41] C. I. Calle, P. J. Mackey, M. D. Hogue, M. R. Johansen, H. Yim, P. B. Delaune, and J. S. Clements, "Electrodynamic Dust Shields on the International Space Station: Exposure to the space environment," *Journal of Electrostatics*, vol. 71, no. 3, pp. 257–259, 2013.

[42] H. K. Elminir, A. E. Ghitas, R. Hamid, F. El-Hussainy, M. Beheary, and K. M. Abdel-Moneim, "Effect of dust on the transparent cover of solar collectors," *Energy Conversion and Management*, vol. 47, pp. 3192–3203, 11 2006.

[43] M. Mani and R. Pillai, "Impact of dust on solar photovoltaic (PV) performance: Research status, challenges and recommendations," *Renewable and Sustainable Energy Reviews*, vol. 14, pp. 3124–3131, 12 2010.

[44] K. L. Mittal and R. Jaiswal, *Particle adhesion and removal*. John Wiley & Sons, 2015.

[45] A. D. Zimon, *Adhesion of Dust and Powder*. Boston, MA: Springer US, 1982.

[46] P. Atten, H. L. Pang, and J.-L. Reboud, "Study of dust removal by standing wave electric curtain for application to solar cells on Mars.," *IEEE Transactions on Industry Applications*, vol. 45, p. 75, 2009.